ChemComm

FEATURE ARTICLE

View Article Online
View Journal | View Issue

Cite this: *Chem. Commun.*, 2026, **62**, 6004

The journey of short peptides: from molecules to materials

Sampurna Routray, Malay Kumar Baroi,† Priyam Das† and Debapratim Das *

Peptide-based supramolecular systems consisting of conserved sets of building blocks and chemical reactions play a crucial role in the fabrication of supramolecular soft materials. Their inherent capacity for self-assembly, biocompatibility, and molecular tunability make them attractive candidates for creating peptide-based materials. This feature article primarily focuses on the modelling strategy of short peptides based on their desired applications. We explored their applications across various areas, including therapeutics, ECM mimics, drug delivery, scaffolds for tissue engineering, chemosensing, creating life-like systems, and in organic electronic devices, to name a few. In this review, emphasis is placed on highlighting the journey of these short peptides from their molecular level to the material state.

Received 9th September 2025,
Accepted 11th February 2026

DOI: 10.1039/d5cc05199a

rsc.li/chemcomm

1. Introduction

Molecular self-assembly refers broadly to the bottom-up formation of hierarchical supramolecular materials through interactions between molecular building blocks, driven mainly by noncovalent forces and, less commonly, by covalent bond formation. Designing such materials requires not only an understanding of the full range of intermolecular interactions but also the ability to precisely tune them to achieve targeted structures and functions. In recent years, self-assembled short peptides have emerged as powerful and versatile building blocks in the development of advanced soft materials.[1,2] These minimalist biomolecules, typically composed of just a few amino acid residues, can spontaneously organise into a wide range of nanostructures, including fibres, tubes, sheets, and hydrogels. The driving force behind these self-assemblies is non-covalent interactions, including hydrogen bonding, π–π stacking, hydrophobic interactions, and electrostatic forces.[3] Despite their structural simplicity, short peptides exhibit a remarkable capacity for functional diversity, tunability, and responsiveness to environmental changes.

As our understanding of peptide self-assembly advances, new strategies are being explored to control their hierarchical

Department of Chemistry, Indian Institute of Technology Guwahati, Assam – 781039, India. E-mail: ddas@iitg.ac.in
† Contributed equally.

Sampurna Routray

Sampurna Routray obtained her BSc degree in Chemistry from the Orissa University of Agriculture and Technology, India, in 2020. She received her MSc degree from the Banaras Hindu University, Uttar Pradesh, India, in 2022. Currently, she is pursuing her doctoral research in the Department of Chemistry, Indian Institute of Technology Guwahati, Assam, India, under the supervision of Prof. Debapratim Das. Her research area includes stimuli-responsive smart soft materials.

Malay Kumar Baroi

Malay Kumar Baroi received his BSc degree in Chemistry from the University of Kalyani, West Bengal, India, in 2019. He completed his MSc degree in Chemistry from the Indian Institute of Technology Guwahati, Assam, India, in 2021. Currently, he is pursuing his doctoral research as a Prime Minister's Research Fellow in the Department of Chemistry, Indian Institute of Technology Guwahati, Assam, India, under the supervision of Prof. Debapratim Das. He works in the research area of Supramolecular Chemical Ligation.

organisation, dynamic behaviour, and multifunctionality, paving the way for next-generation soft materials that are both smart and sustainable. The availability of various functional groups as side-chain functionalities of amino acids (natural and synthetic), in combination with proper design and folding of the synthesised peptides, also allows one to create small peptide assemblies for targeted applications. Their inherent biocompatibility, ease of synthesis, and modularity make them particularly attractive for applications across biomedicine, tissue engineering, drug delivery, sensing, organo-electronics, and nanotechnology, to name a few. Furthermore, their ability to mimic features of the extracellular matrix (ECM) and facilitate cell adhesion and signalling has placed them as key candidates in the design of bioinspired materials.

Such peptides, when appropriately designed, have emerged as attractive alternatives to proteins and longer peptides across a range of applications. Our group has focused on designing hierarchical assemblies of short peptides, particularly peptide amphiphiles (PAs), and has developed peptide-based assemblies and hydrogels for various applications, including organocatalysis, drug delivery, sensing, tissue engineering, water remediation, organoelectronics, and transient life-like systems. The breadth of research in this field necessitates a concise overview of progress to date, alongside an outlook on future directions. While recent review articles offer valuable insights into peptide- and protein-based systems, many of them primarily focus on the self-aggregation behaviour and mechanism of peptides.[2,4–8] In contrast, in the present feature article, we restrict our discussion to short peptides (2–10 amino acids), with a major emphasis on the diverse applications enabled by these small peptide systems. For the ease of reading, Charts 1 and 2 present the chemical structures of the peptides discussed, and Table 1 summarises their self-assembled architectures and corresponding applications.

2. Self-assembling short peptides: from sequence to application

2.1. Design principle

When designing short peptides for a targeted application, the peptide's primary sequence, particularly the choice of amino acids, is the first aspect to consider. With the wide variety of geometric structures, side-chain polarities, hydrogen bonding tendencies, ionised states, and functional groups present among amino acids, it is essential to select the appropriate amino acids for the peptide sequence. For example, in many applications, aqueous solubility is essential, and to achieve solubility at neutral pH, the incorporation of Lys into the sequence is beneficial, as its pK_a ($\sim$10.5) keeps the side-chain amine protonated at neutral pH. On the other hand, introducing amino acids with side-chain carboxylic acid functionality requires a basic pH for solubilisation, whereas Arg adds a permanent charge to the peptide. All these amino acids in a peptide work cooperatively to provide the required supramolecular interactions, such as hydrophobic interactions, π–π stacking, hydrogen bonding, ionic interactions, and metal-ion coordination. These interactions are crucial for achieving the desired secondary structures required for self-assembly. For example, Ile shows stronger β-sheet hydrogen bonding propensity and hydrophobicity compared to that of Leu.[54] Proline, having a ring structure and no hydrogen bonding possibility, is not favoured for β-sheet peptides. However, the ^{D}Pro-^{L}Pro segment is successfully utilised for β-hairpin generation.[55]

The sequence modification, with N- or C-terminal protection or the attachment of application-based groups, is important. For short peptides, as few interactions are possible, appropriate terminal protection helps provide the required aromatic stacking and hydrogen bonding. Moreover, the desired applications may also demand the attachment of such groups. The attachment of these groups can also be done on the side chains of the peptide sequence, depending on the application. For example,

Priyam Das

Priyam Das earned his BSc degree in Chemistry from the University of Calcutta, India, in 2018. He received his MSc degree in Chemistry from the Indian Institute of Technology Guwahati, Assam, India, in 2020. Currently, he is pursuing his doctoral research as a Prime Minister's Research Fellow in the Department of Chemistry at the Indian Institute of Technology Guwahati, Assam, India, under the supervision of Prof. Debapratim Das. His research area includes non-equilibrium supramolecular self-assemblies.

Debapratim Das

Debapratim received his PhD in 2007 from the Indian Association for the Cultivation of Science, where he worked on membrane mimetic systems. He was subsequently awarded a Humboldt Fellowship and joined the Max Planck Institute for Molecular Physiology, Dortmund, Germany, to conduct research in chemical biology. Subsequently, he moved to the University of Cambridge to work on host–guest chemistry. In 2011, Dr Das joined the Department of Chemistry at the Indian Institute of Technology Guwahati, and he has been serving as Professor since 2019. His current research centres on supramolecular dynamic aggregates.

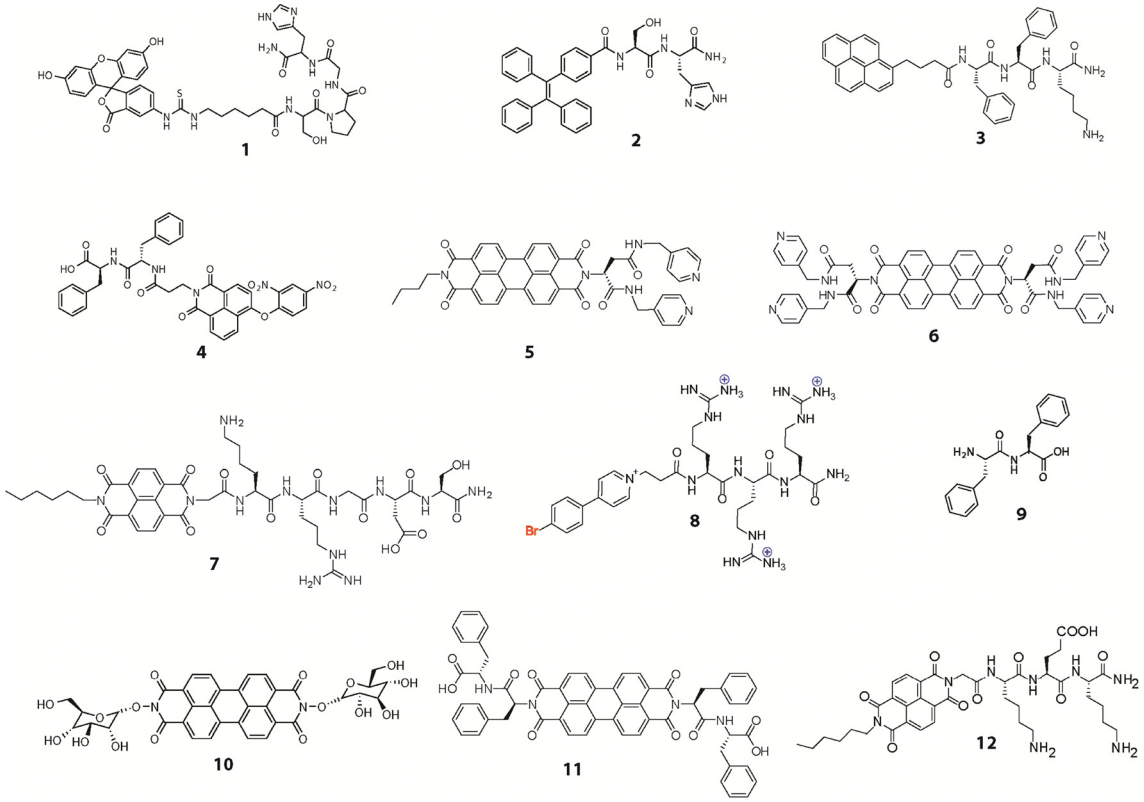

Chart 1 Molecular structures of peptides used as chemosensors and for organic electronics applications.

Fmoc, derivatives of naphthalene, phenothiazine, carboxybenzyl, azobenzene, and pyrene are examples of aromatic groups that are successfully used to create self-assembling short peptides. Attachment of long hydrocarbon chains to either terminal to create PAs is another important strategy.[56] By achieving this, the desired hydrophilic–lipophilic balance (HLB) of the short peptide is attained, leading to effective self-assembly. Similarly, the attachment of chromophoric groups, such as pyrene, arylene diimides (ADIs), coumarin, dansyl, anthracene, and rhodamine, is required when designing chemosensors.[57] In the case of peptide-based drug delivery systems, ligands to the overexpressed receptors of the targeted cells/tissues are often attached to the peptide sequence.[8] In this context, altering the chirality of a peptide provides significant protection from proteolytic enzymes because most biological proteases are highly stereoselective for L-amino acid chains.[58]

Smart materials are advanced materials that can significantly change their properties (shape, colour, stiffness, *etc.*) in a controlled manner in response to external stimuli, such as temperature, light, pH, or electric fields. For short peptides, the response to a change in pH can be easily achieved by incorporating amino acids such as His, Lys, Asp, or Glu through fine-tuning the sequence.[59] To incorporate light-responsive behaviour, the peptides can be functionalized with light-responsive azobenzene, spiropyran or light-cleavable nitroveratryl or similar groups.[60] Similarly, redox-response can be achieved by incorporating Cys residues that can form disulfide linkages and respond to biomolecules like glutathione (GSH). To create a 3D cell culture medium, a 3-dimensional network that mimics the ECM is essential. To provide such a network with short peptides, the peptide must be designed in a manner that allows it to self-assemble in a hierarchical fashion to form a hydrogel. This can be achieved by maintaining an appropriate HLB, incorporating amino acids that provide optimum solubility in water, as well as hydrogen bonding sites and aromatic groups that allow π−π stacking. Multicomponent assembly is another approach wherein a non-assembling sequence or other molecule is combined with a self-assembling sequence. Even two self-assembling sequences can also be mixed together to achieve the final required property.

In this context, Artificial intelligence (AI) and machine learning (ML) are evolving as powerful tools for the rational design of peptides tailored to specific applications.[61,62] By learning patterns from large datasets of peptide sequences, structures, and experimentally measured properties, ML tools can predict key characteristics such as self-assembly propensity, secondary structure, stability, bioactivity, toxicity, and cell permeability. Generative models further enable the creation of novel peptide sequences optimised for predefined targets, while multi-objective optimisation allows for the simultaneous balancing of competing parameters, such as activity, stability, and solubility. Coupled with high-throughput synthesis and experimental validation, AI- and ML-guided design can significantly reduce trial-and-error, accelerate discovery, and expand the accessible chemical space for functional short peptides.

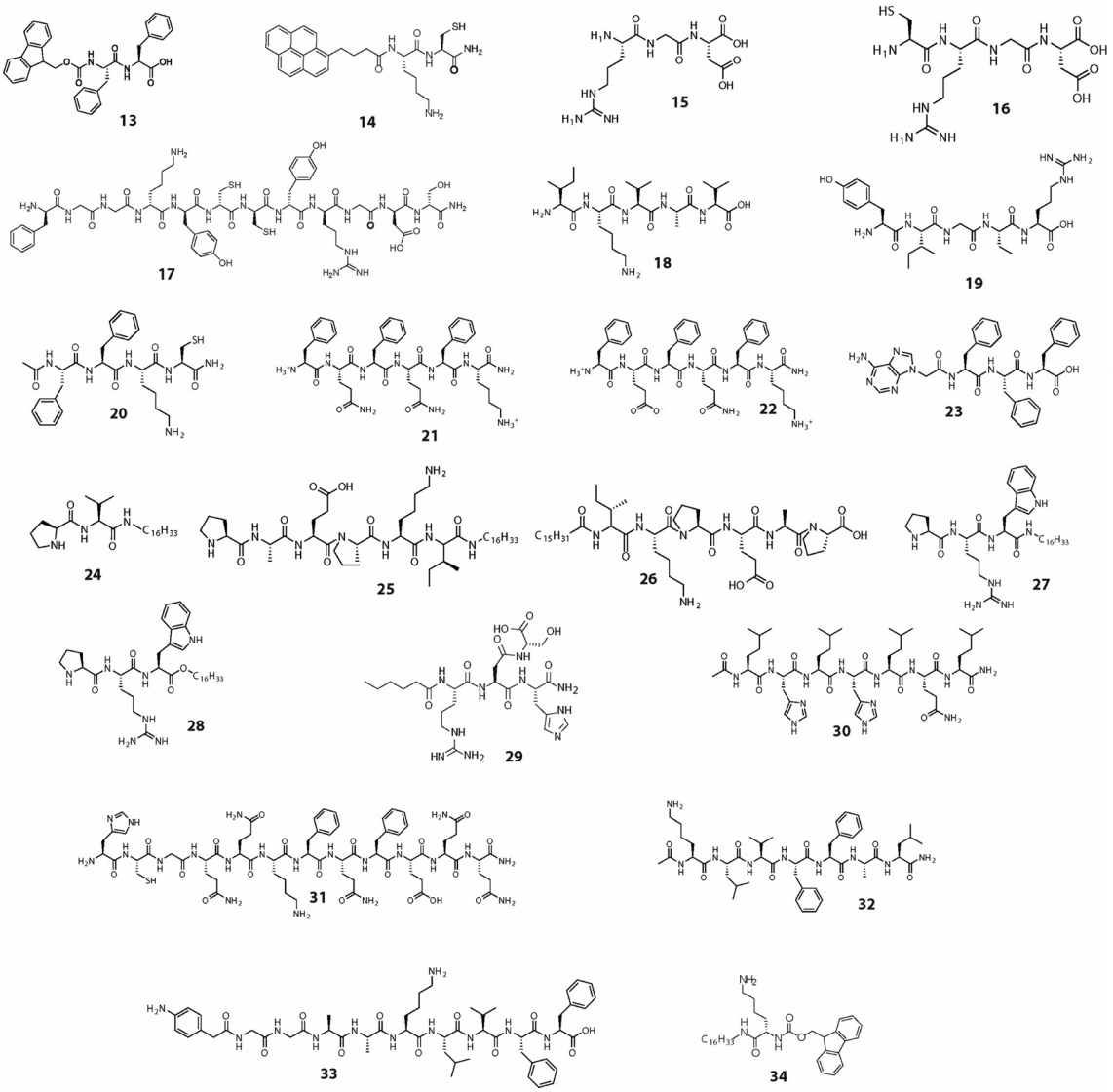

Chart 2 Molecular structures of peptides used for biomedical, catalysis and other applications.

The design strategies for short peptides span multiple dimensions and are largely dictated by the intended application. A schematic flowchart illustrating the progression from peptide design to application is presented in Fig. 1. Several excellent recent reviews comprehensively discuss the design principles governing self-assembling peptides, providing valuable insights into this rapidly evolving field.[63,64]

2.2. Self-assembly driven chemosensing

Essentially, a chemosensor functions as a molecular probe that, upon binding with the analyte, generates a detectable signal. The signals could be a change in the visible colour, luminescence, or an electric signal.[65–67] Supramolecular aggregation between molecules offers ample opportunities for designing and developing new chemosensors. The reversible processes of aggregation and disaggregation generate detectable signals that can be readily quantified and correlated with the analyte concentration.

2.2.1. Emissive chemosensors. Sequence-dependent recognition is one of the main advantages of short peptide-based chemosensors. The binding affinity and selectivity toward target analytes, such as metal ions, anions, small organic molecules, and biomolecules, can be significantly changed by minute changes in amino acid composition, chirality, and terminal functionalities. Analyte recognition relies heavily on noncovalent interactions, such as hydrogen bonding, electrostatic forces, π–π stacking, and metal coordination, which frequently convert molecular binding events into quantifiable optical or electrical signals.

Chromogenic groups and analyte-binding motifs can easily be attached to the peptide that forms aggregates with the specific analytes. The aggregation leads to certain changes in the electronic environment around the chromogenic groups, thereby producing a signal (turn on or off) that can be correlated with the analyte concentration. A number of photophysical mechanisms for fluorescent probes, like photo-induced

Table 1 Self-assembled nano-structures formed by different short peptides and their applications discussed in this article

Peptide Number	Medium/solvent/condition	Nanostructure formed	Application	Ref.
1	Water	—	Cu^{2+} and H_2S sensing	9
2	10 mM phosphate buffer pH 7.4	—	Hg^{2+} sensing	10
3	1 : 1 ACN–water	Fiber	Picric acid sensing	11
4	Water	Fibrous network	Imaging and apoptosis induction in cancer cells by utilizing endogenous hydrogen sulfide	12
5	1 : 1 DMF–water in the presence of Pd^{2+}	Sphere	Pd^{2+} and CN^- sensing	13
6	MeOH	Sphere	Picric acid sensing	14
	MeOH in the presence of picric acid	Tape		
7	Water	Fibrous network (hydrogel)	Intracellular pH sensing	15
8	Phosphate buffer pH7, CB[8], heparin	Sphere	Heparin and protamine sensing	16
9	Electric field growth	Microrod	Piezoelectric power generator	17
10	Water–DMF	Nanoribbon and nanotape	Organic electronic	18
11	THF	Helical fiber	Organic electronic	19, 20
	THF–Water	Nanoring		
	HFIP	Sphere		
	MeOH	Sphere		
	ACN	Sphere		
	Acetone	Sphere		
	Chloroform	Fiber		
	THF	Fiber		
12	Water	Fibrous network	*p*-Xylene gas sensing	21
13	Water	Fibrous network	Protection of oxygen-sensitive enzymes	22
	Water pH 7.5 and PLL-SH	Hydrogel	Triggering antitumor immune response	23
14	Water	Fibrous network	Asymmetric disulfide synthesis	24
	TRIS buffer pH 8	Fibrous network	Enzyme protection	25
	TRIS buffer pH 8, surface coating with 5-ACl and BPEI. Functionalized with Au-nanostructures	Core–shell bead	Drug delivery	26
			Tissue engineering	27, 28
			Transient coacervation	29
			Dye degradation, uric acid detection, water remediation	30–32
15	Buffer	Hydrogel	Vascularization and tissue repair	33
16	Buffer, PEDOT	Film	Regeneration of damaged sciatic nerves	34
17	Water, CB[8], HRP	Nano particle	3D cell-proliferation of Raw 264.7 macrophages	35
18	buffer	Spheroids	Cell proliferation of neural stem cells	36
19	Buffer	Hydrogel micropatterns	Nerve regeneration	
20	TRIS buffer pH 8	Fibrous network	3D cell-proliferation	37
21 and 22	PBS 2×	Hydrogel	Protein delivery	38
23	Water	Hydrogel	Drug delivery	39
24	Water	Hydrogel	Aldol reaction	40
25 and 26	Water	Hydrogel	Nitro-aldol reaction	41
27 and 28	Water	Hydrogel	Nitro-aldol reaction	42
29	Water	Micelle	Hydrolase mimic	43
30 and 31	Water	Fibers	Esterase like activity	44, 45
32	ACN–water	Nanotube	Retro Aldol catalysis	46
33	Water	Fibril	Electrocatalysis of O_2 reduction	
34	Water	Helical fiber (hydrogel)	Hollow silica nanotube synthesis	47
35	Water	Hydrogel	Transient hydrogel	48
36	Buffer	Hydrogel	Transient hydrogel	49
37	Buffer	Hydrogel	Transient hydrogel for information encryption	50
38	50 mM HEPES pH8	Coacervate	Transient coacervation	51
40	Water, CB[8]	Vesicle	Transient vesicle	52
41	Water, CB[8]	Vesicle	Self-abolishing transient vesicle	53

electron transfer (PET), resonance energy transfer (RET), and intramolecular charge transfer (ICT), excimer formation *etc.* have been reported. Based on these strategies, several chemosensors utilising a variety of fluorogenic groups have been designed for various important analytes.[57]

The design principle for a chemosensor involving such a signal transduction mechanism includes three components: a fluorophore, a linker and a receptor.[57] A classic example of signal transduction upon analyte binding was reported by Tang *et al.*[9] Peptide **1** was designed by connecting the fluorophore (fluorescein isothiocyanate) to the ionophore His-Gly-Pro-Ser through a hydrophobic linker. Upon binding with Cu^{2+}, the initial fluorescence quenches, providing a ''turn-off'' signal. The Cu^{2+} bound sensor was highly selective toward H_2S, and

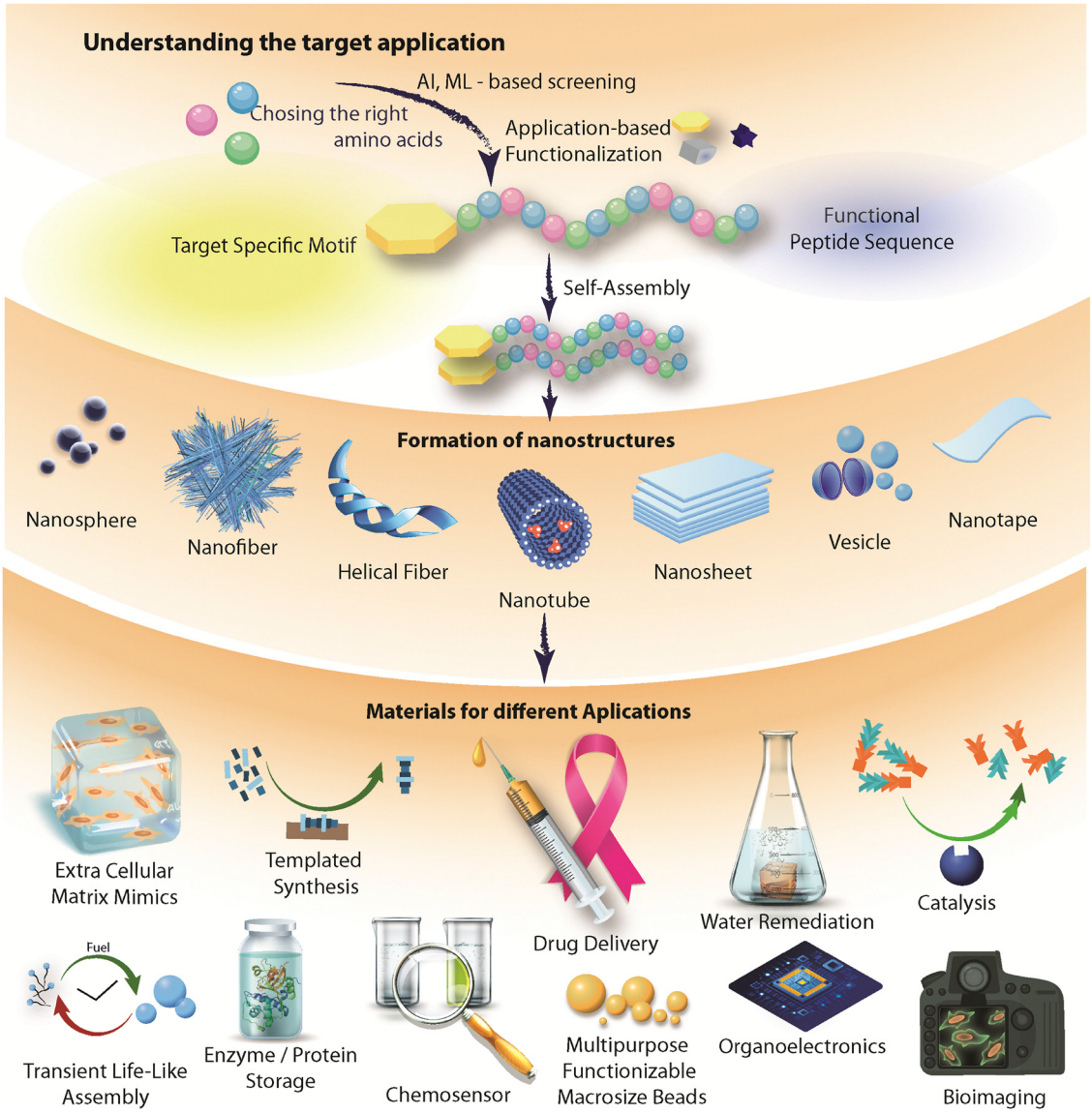

Fig. 1 Schematic illustration of the hierarchical peptide self-assembly to different nano-structures and for various applications.

the presence of H_2S led to the recovery of the emission, thereby making the sensor act as a "turn-on" sensor for H_2S. The chemo-sensor can detect naturally occurring H_2S within HeLa cells and zebrafish larvae. A plethora of similar fluorescent chemosensors have been reported in the literature, and it is beyond the capacity of this article to discuss about them in detail.

As mentioned earlier, self-assembly- and disassembly-induced changes in the emission property can also be utilised to develop chemosensors. Lee *et al.* utilised the aggregation-induced emission (AIE) of tetraphenylethylene (TPE) to efficiently detect ions.[10] TPE was connected to the Hg^{2+} binding motif, Ser-His (**2**). The binding of the analyte triggered the AIE effect of TPE, thereby enhancing fluorescence (Fig. 2A). Charge transfer (CT) complex formation between an electron-rich fused aromatic moiety and an electron-deficient group has also been exploited to create an efficient sensor. Peptide **3** was designed by attaching pyrene to the well-established self-assembling unit "Phe–Phe" followed by a Lys to achieve the required solubility.[11] The Phe–Phe unit exhibits self-assembling propensity, and through self-assembly, the pyrene units form π–π stacking, resulting in excimer emission (Fig. 2B).[68] In the gel state, detection relied on the excimer band of pyrene. In the presence of picric acid (PA), the CT complex formed between pyrene and PA that quenched the excimer emission (Fig. 2C). On the other hand, in the solution state, sensing was based entirely on the monomer emission of pyrene. In the sol state, the peptide molecules existed in a non-aggregated form, showing only monomeric emission. When PA was introduced, the CT complexation resulted in a sharp reduction in the emission intensity of the monomer (Fig. 2D). The detection limits were found to be 115.24 ppt and 22.91 ppb in the sol and gel states, respectively. The gel-coated paper strips also showed a reduction in the excimer emission in the presence of nitrophenols, thereby

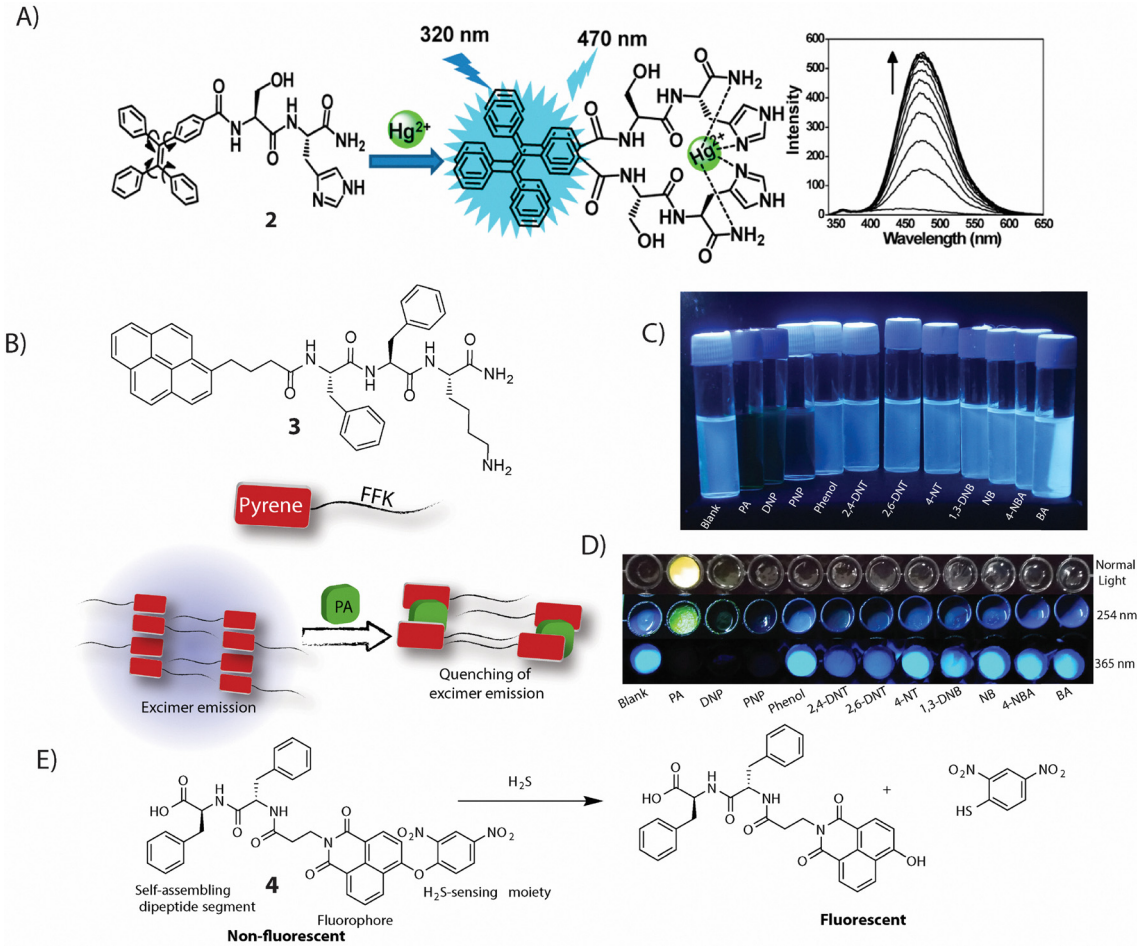

Fig. 2 (A) Proposed binding mode of **2** with Hg^{2+}. (B) Graphical presentation of the aggregation of PyFFK and picric acid detection mechanism. (C) The change in emission of PyFFK in the presence of picric acid in (C) solution and (D) gel state. (E) Proposed mechanism of H_2S sensing by peptide **4**. Adapted/reproduced with permission from ref. 10–12. Copyrights 2016 and 2019 American Chemical Society and 2021 Royal Society of Chemistry.

selectively detecting picric acid at a femtogram level with a minimum detection limit of 11.45 fg cm^{-2}.

Due to their outstanding photochemical stability and high quantum yields, arylenemono- and diimides have been extensively used in the design of new chemosensors.[69,70] For example, Verma *et al.* reported a naphthalene monoimide (NMI) functionalized Phe–Phe peptide (**4**).[12] The diphenylalanine segment is responsible for the self-aggregation, the NMI provides fluorescence, and the dinitrophenyl group acts as the sensing group (Fig. 2E). The initially non-emissive peptide undergoes a chemical transformation in the presence of H_2S and becomes emissive. It is successfully activated by endogenously produced H_2S of cancer cells and could be applied for specific imaging of cancer cells.

Similarly, peptides **5** and **6** were designed to utilise analyte-binding-driven assembly–disassembly, with the consequent changes in emission used for sensing.[13,14] Probe **5** exhibited high selectivity toward Pd^{2+} ions over other metal cations, with a sensitivity of 0.55 ppb – significantly lower than that of comparable chemosensors.[13] Binding with Pd^{2+} induced aggregation of the ligand, leading to quenching of its emission. This quenched emission can be restored in the presence of CN^- ions, as cyanide forms a stronger complex with Pd^{2+}, leading to the disaggregation of the system. The sensor displayed exceptional selectivity for CN^-, with a detection limit as low as 0.226 ppb. The tetra-pyridine containing probe, **6**, was found to be an efficient sensor for picric acid.[14] The probe displayed typical aggregation-caused quenching (ACQ) behaviour and exhibited a fluorescence "turn-off" response toward picric acid. The response was found to be unaffected by the presence of other interfering nitroaromatic compounds. The sensing mechanism involved hydrogen bonding between picric acid and the pyridine groups of **6**, inducing the aggregation of the probe into higher-order, tape-like structures and consequent emission quenching. The probe demonstrated a low detection limit of 5.6 nM (1.28 ppb) and a remarkably high Stern–Volmer constant of 6.87×10^4 M^{-1}.

Utilising the intrinsic emissive behaviour of naphthalene diimide (NDI),[71] DI PA (**7**) was designed for cellular internalisation and local pH sensing.[15] The asymmetric PA was designed by attaching a C_6H_{13}-alkyl chain to one end of the NDI moiety, while a GKRGDS sequence was connected to the other. The RGDS fragment has been purposefully introduced for tumour

homing and cell adhesion properties and, henceforth, to play the dual role of a structural component as well as a biological ligand.[72] Under physiological conditions, **7** efficiently self-assembled into a self-supporting hydrogel. The presence of two positively charged amino acid residues (Lys and Arg) and one negatively charged amino acid (Glu) in the peptide-conjugate induced pH responsiveness in the system, as the gel dissolved under acidic conditions. At higher pH, due to the strong π–π stacking of the NDI groups, a broad emission peak centred around 500 nm appeared, which disappears under acidic conditions. The peptide also showed easy internalisation within RAW264.7 cells and was found to be noncytotoxic. The pH-responsive emission behaviour was further utilised to determine the pH at different cellular locations.

Although fluorescence-based sensing probes are widely used, they face limitations such as photobleaching, autofluorescence, and potential phototoxicity. Supramolecular phosphorescence sensing offers advantages, including millisecond lifetimes, large Stokes shifts, and minimal background interference; yet, RTP-based probes remain relatively underexplored, particularly in solution.[73]

In this regard, our group has developed a cucurbituril[8] (CB[8])[74–76] based room-temperature phosphorescent sensing probe (BPR@CB[8]) that can be used to detect heparin and protamine under physiological conditions (Fig. 3A).[16] An Arginine-rich 4-(4-Bromophenyl)-pyridine (BP) derivative (BPR, **8**) was synthesised.[77] In the presence of CB[8], a 2 : 1 homoternary complex[78] (BPR@CB[8]) is formed that produces a minor phosphorescence due to supramolecular confinement of the BP unit. In the presence of heparin, BPR@CB[8], which has multiple positive charges, forms a nano-assembly through electrostatic interactions, thereby significantly enhancing its phosphorescence (Fig. 3B). This "turn-on" emission proves to be the key to sensing heparin. Excellent selectivity toward Heparin

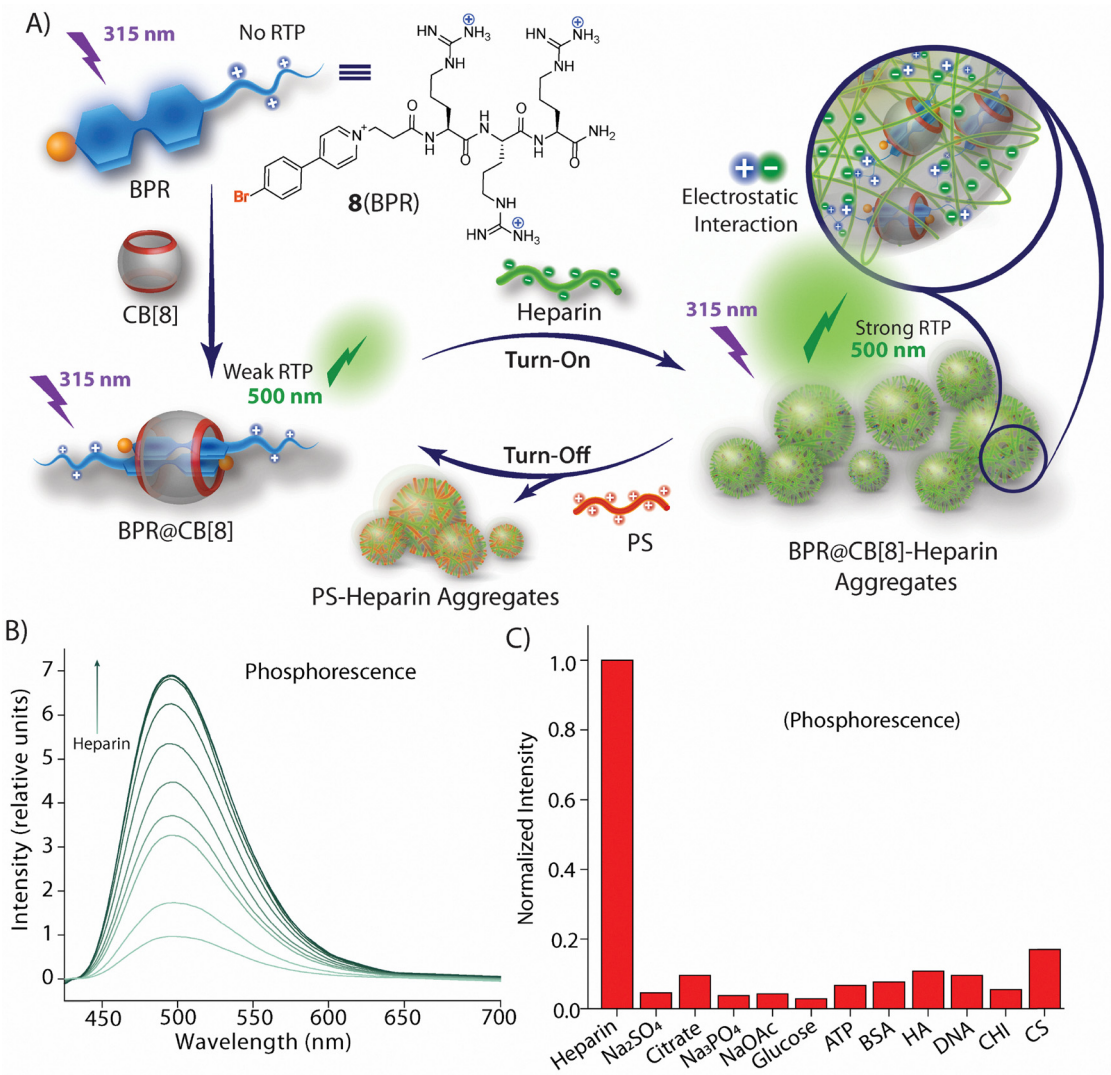

Fig. 3 (A) Schematic presentation of the sensing mechanism of Heparin and PS using BPR@CB[8]. (B) Heparin sensing: the enhancement of phosphorescence when BPR@CB[8] was titrated with increasing concentration of Heparin. (C) Selectivity of the BPR@CB[8] toward heparin over various other negatively charged molecules. Reproduced with permission from ref. 16. Copyright 2025 American Chemical Society.

was obtained when compared to other anionic probes (Fig. 3C). The reverse assembly mechanism was applied to efficiently detect Protamine sulfate (PS), the antidote of heparin. With several arginine residues, PS had a higher affinity toward Heparin compared to BPR@CB[8]. When added to the Heparin-BPR@CB [8] solution, it displaces BPR@CB[8] through binding with Heparin, and consequently, ''turn-off'' phosphorescence sensing of PS was achieved. Further, the detection limits for heparin and protamine were determined to be 61 and 82 ng mL^{-1} in 10% HBS, respectively. The phosphorescence sensing of both analytes was found to be effective in biofluids such as human blood serum (HBS) and human urine (HU).

Despite these developments, challenges still remain. Ongoing concerns include enhancing long-term stability under physiological and environmental conditions, as well as achieving high selectivity in complex, real-world environments. Furthermore, further experimental and theoretical research is needed to fully understand the mechanistic relationship between molecular recognition and supramolecular reorganisation. In the future, exciting opportunities will arise to integrate short peptide chemosensors with wearable or implantable devices, smart materials, and microfluidic platforms. It is anticipated that developments in machine learning-guided sequence optimisation and computational peptide design will further accelerate discovery. All things considered, short peptide-based chemosensors offer a flexible and promising platform that connects functional materials and molecular recognition for next-generation sensing applications.

2.3. Short peptides in organic electronics

The growing demand for environmentally friendly organic semiconductors that are easily fabricated and tunable has motivated the development of self-assembling peptide nanostructures with enhanced semiconducting properties.[79] Recently developed bio-inspired peptide semiconductors exhibit a wide range of supramolecular morphologies with diverse optical and electrical characteristics. These peptide assemblies have also been explored for applications in piezoelectric devices and ultrasensitive electrochemical sensors.

Aromatic short peptides are the most widely studied self-associating systems for semiconducting nanomaterials.[7] Diphenylalanine (FF, **9**), a minimal aromatic dipeptide derived from β-amyloid (Aβ), forms diverse semiconducting supramolecular architectures.[7] Its self-assembly can be modulated through the choice of solvent, external fields, and controlled solute convection, enabling the formation of aligned nanotubes and ordered nanoarrays with varied morphologies. Notably, these superstructures share an identical crystallographic lattice, indicating that complex architectures can be achieved through the simple control of the dewetting process.[79] Studies show that FF dimers act as quantum dot-like building blocks during self-assembly. The aggregation proceeds through multiple supramolecular phases driven by T-shaped aromatic stacking, head-to-tail interpeptide interactions, and peptide–water hydrogen bonding.[80] This process yields porous nanotubular crystals featuring amide backbone channels surrounded by ''zipper-like'' aromatic interlocks, which promote π-electron delocalisation.[79] Importantly, the reversible transformation between quantum dots and nanotubes controlled by solution conditions, such as concentration and solvent, underpins the semiconductivity of FF assemblies. Using these FF nanotubes, several devices have been successfully constructed for light-induced electricity generation, biosensing, energy storage *etc*.[79,81–83] For example, Yang *et al.* reported the microrod array of FF peptide utilized for piezoelectricity generator. Fig. 4A shows the prototypical generator using vertical FF arrays as a direct source of power for an LCD. The open-circuit voltage and short-circuit current obtained from this generator upon multiple tapping is shown in Fig. 4B.[17]

To this end, arylenemono and diimides are well-established as n-type organic semiconductors. Numerous studies have been conducted to explore their conductive characteristics and their applications in organic electronic devices.[84] It has been found that the aggregation of these semiconductors plays a significant role in influencing their electrical characteristics and overall performance.[84] Rybtchinski and co-workers demonstrated the kinetically controlled self-assembly of perylene diimide (PDI) – peptide conjugates to form various organic nanostructures in a stepwise manner.[85] In a similar study, Faul *et al.* synthesised a symmetric sugar–PDI conjugate (**10**) and studied its aggregate morphologies and formation mechanisms in detail in the mixed solvent system water/*N*,*N*-dimethylformamide (H_2O/DMF) with varying volume ratios.[18] The peptide self-assembled into planar ribbons in both 20% and 40% water in DMF (Fig. 4C and D). However, the supramolecular chirality of these ribbons was found to be opposite. Interestingly, only left-handed helical nanofibers were obtained in 60% and 80% water in DMF (Fig. 4E and F). Experimental evidence, combined with DFT calculations, suggests that kinetic and thermodynamic factors play key roles in tuning the structures and helicity. The self-assembled structures were further investigated for their gas-sensing properties. Devices based on single nanoribbons for hydrazine sensing exhibit better performance than nanofiber bundles (Fig. 4G and H).

A similar pathway-dependent self-assembled nanostructure and consequently the semiconducting property were observed for peptide **11**.[20,86] In THF, right-handed helical fibres were formed, while in a 10% THF–water solution, the morphology changed to nano-rings with a switch in helicity to left-handedness. A combination of experimental results and DFT calculations revealed that both thermodynamic and kinetic factors play a pivotal role in directing these differential self-assembly processes. In THF, right-handed helical fibres are formed in a kinetically controlled fashion. On the other hand, in the case of 10% THF–water, the initial nucleation of the aggregate is controlled kinetically. Due to the molecule's differential solubility in the two solvents, elongation of the nuclei into fibres was arrested beyond a critical length, resulting in nanoring formation governed by thermodynamic control. Importantly, the helical fibres showed superior semi-conducting property to the nano-rings as confirmed by conducting-AFM and conventional *I–V* characteristics. The same peptide (**11**) exhibited a fibre-like structure when dissolved in nonpolar solvents such as THF and $CHCl_3$, whereas it demonstrated a spherical morphology

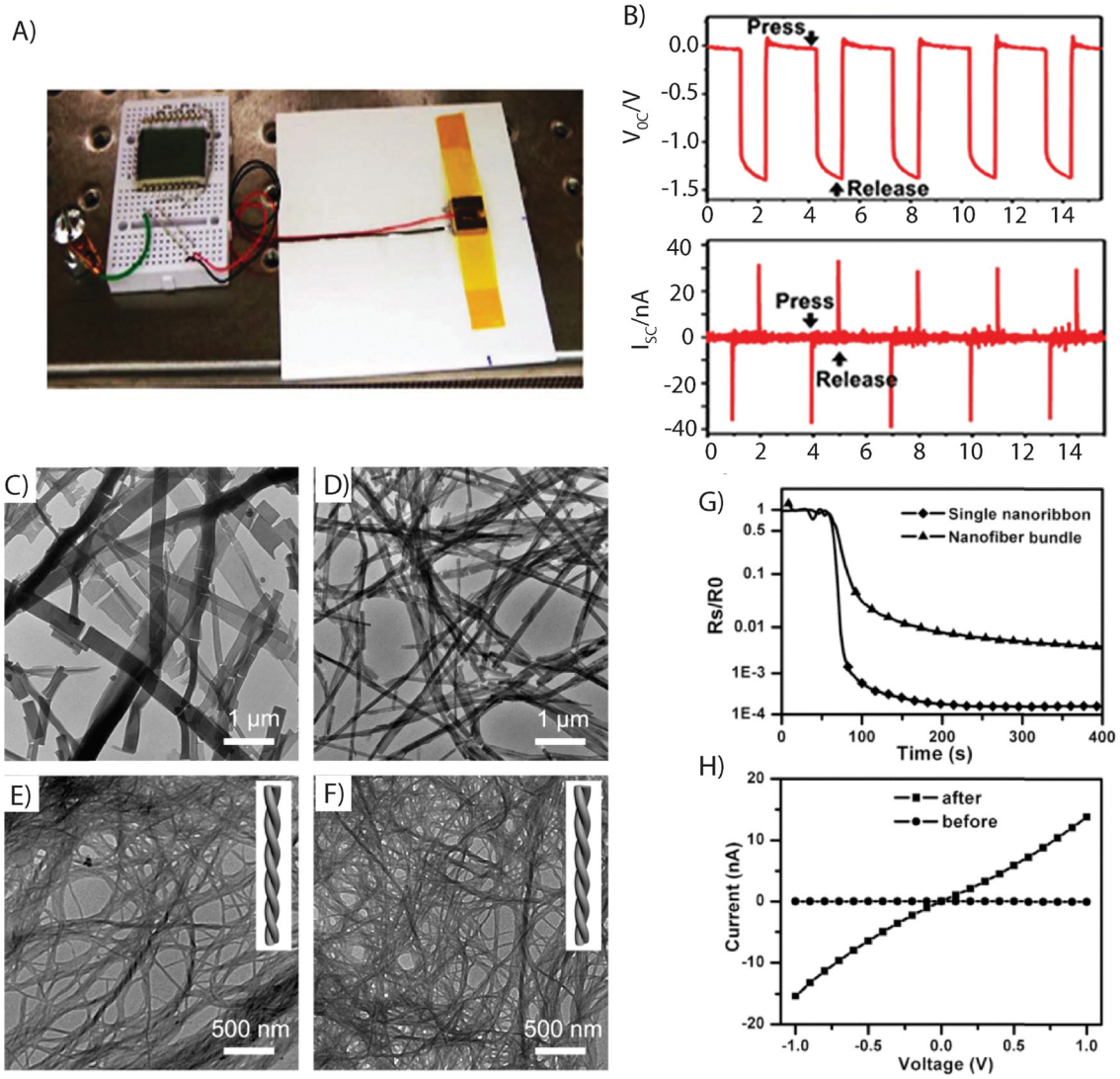

Fig. 4 (A) Photograph of the prototypical generator using vertical FF arrays as a direct power source for an LCD. (B) Open-circuit voltage (top) and short-circuit current (bottom) from the generator in (A). (C)–(F) TEM images of **10** (0.06 mg mL^{-1}) nanostructures obtained from (C) 20%; (D); 40% (E) 60% and (F) 80% water in DMF. The inserts in E and F indicate the left-handed helical sense of the nanofibers. (G) sensing properties of devices prepared from a single nanoribbon and bundled nanofibers, 10 minutes after the injection of hydrazine. (H) *I*–*V* curves of the nanoribbon before and after the injection of hydrazine. Nanofibers and nanoribbons were obtained from 60 and 40% water in DMF, respectively. Reproduced with permission from ref. 17 and 18. Copyrights 2016, Springer Nature and 2012 WILEY-VCH Verlag GmbH & Co. KGaA, Weinheim.

in more polar solvents like HFIP, MeOH, ACN, and acetone.[19] The direct current (DC) of nanostructures (spheres and fibres) remained relatively constant, whereas the alternating current (AC) displayed variation in the low-frequency range. The impedance characterisation has also been used to assess the AC conductivities of the nanostructures. A frequency scan from 20 Hz to 2 MHz was applied to measure the AC conductivities of the PDI-peptide conjugate in the presence of different solvents.

Further, we have utilised the conducting properties of ADI-peptide conjugates for gas sensing. Considering the significant risks associated with inhaling harmful volatile organic compounds (VOCs) found in the environment, it is necessary to develop a portable monitoring device. In this regard, a shorter analogue of ADIs, NDI, being electron-deficient, has demonstrated effective binding to aromatic compounds through a charge-transfer interaction.[87] We anticipated that aromatic VOCs could similarly interact with the NDI group and produce a measurable electrical signal. Hence, an NDI-peptide-based conjugate, **12**, has been developed for an ultrafast, selective, and efficient detection of *p*-xylene at room temperature (Fig. 5).[21] A short self-assembling peptide sequence (KEK) was attached to NDI, resulting in the formation of supramolecular polymers with an ordered arrangement of the NDI core. These aggregates thereafter underwent elongation along the long axis to form nanofibers. The nanofibers thus formed enabled the attainment of semiconducting properties due to the ordered stacking of the NDI groups. Additionally, we doped the system with conductive carbon dots (CD) to enhance the conductivity of the

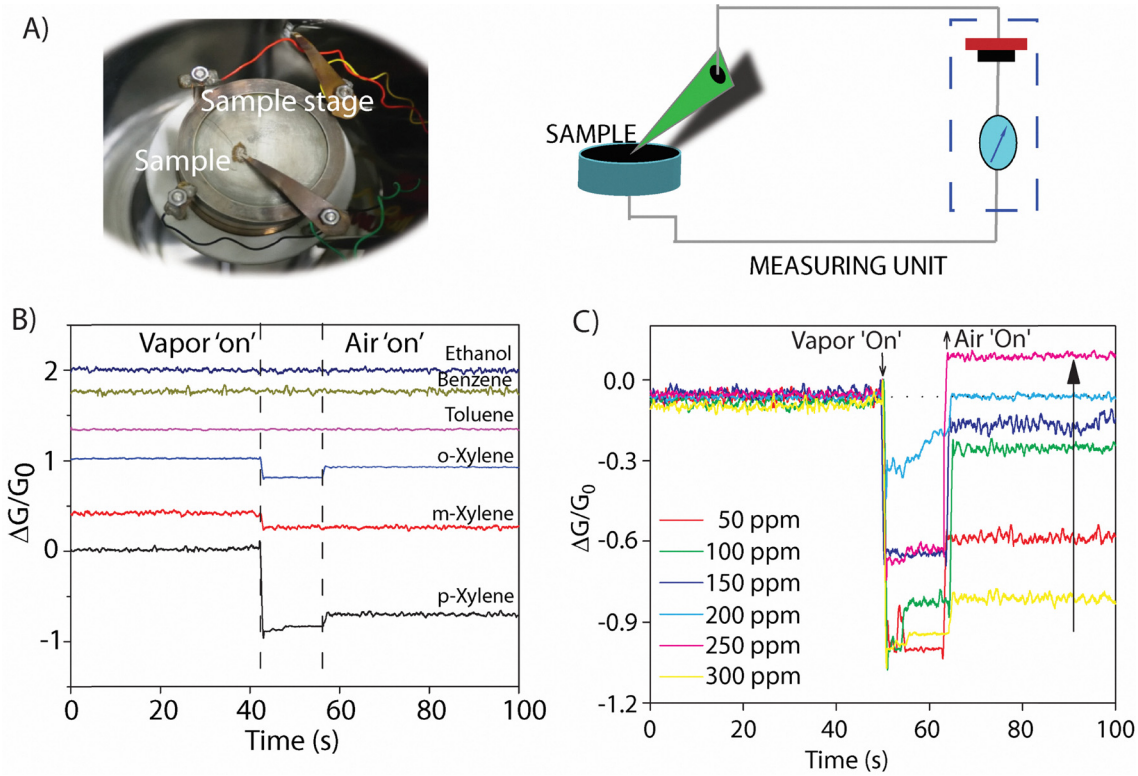

Fig. 5 (A) Experimental arrangement for gas-sensing measurements with circuit diagram. Conductance change ($\Delta G/G_0$) of the sensor developed from **12** with (B) different VOCs (50 ppm) and (C) with varying concentrations of *p*-xylene. Reproduced from ref. 21. Copyright 2018, American Chemical Society.

sensing material as a whole. A device was fabricated by combining PVA, **12**, and CD for sensing purposes (Fig. 5A). The device specifically detected *p*-xylene in the presence of different other VOCs (Fig. 5B). The detection limit for *p*-xylene was found to be 50 ppm, yielding a response of 96% (Fig. 5C). Moreover, the sensor also demonstrated successful application in crude oil, with its rapid detection of VOCs at ambient temperature being a significant advantage over other sensors reported.

Peptide-based systems offer several benefits, including solution processability, environmental responsiveness, and structural adaptability, despite their intrinsic conductivity being lower than that of conventional organic semiconductors. Despite all these advantages, peptide-based organic electronic devices remain relatively rare. These semiconducting systems can be incorporated in next-generation organic electronic devices, especially in wearable electronics.[88,89] With the advancement of peptide design strategies and hybrid peptide-organic architectures, there is significant potential in this area that warrants further exploration in the future.

2.4. Self-assembled peptides for biomedical applications

Because self-assembling peptides can incorporate diverse functional domains such as cell-adhesion motifs, signalling sequences, vaccine epitopes, and therapeutic moieties, they enable the formation of complex nanostructures with broad biomedical applications. In this section, an overview of the literature will be provided on recent studies on peptide self-assembly for applications in platforms for cell proliferation, drug delivery, and protective envelopes for biomolecules.

2.4.1. Peptide-hydrogel as a protective envelope for enzymes. Proteins utilise a variety of supramolecular interactions to attain their optimal three-dimensional structures, a process known as protein folding.[90] In the case of enzymes, proper folding creates the reactive pocket required for substrate binding. Even minor environmental changes, such as a rise in temperature or a change in pH, can trigger unfolding, leading to denaturation or loss of activity.[91] It is a challenging task to protect enzymes from denaturation while keeping them under ambient conditions. Several methods, including immobilisation on solid supports and the use of chaperones, have been utilised to protect proteins from denaturation.[92–94] However, there are several limitations, including the shorter shelf life of enzymes under adverse conditions.

Hydrogels have also been used to protect enzymes from denaturants. Abramhovich *et al.* demonstrated that Fmoc-FF (**13**) hydrogels can selectively encage O_2 and restrict its diffusion beyond the inherent gas-barrier properties of gels, without requiring metal-ion binding.[22] Importantly, O_2 encaging in Fmoc-FF gels was shown to passively protect the O_2-sensitive enzyme HydA1, enabling sustained hydrogen production, even when the hydrogel was prepared in aqueous buffer. Similarly, on several occasions, protein-based hydrogels have been utilised for effective biocatalysis or as a nanocarrier.[95,96] An exciting opportunity emerged to apply one of our peptide-based hydrogelators,

PyKC (**14**), for this purpose.[24,25] Unlike other supramolecular hydrogels, the PyKC-hydrogel remained insoluble in water, most of the water-miscible organic solvents, and, importantly, in human blood serum (HBS) for more than three years. However, disulfide bond breakers such as glutathione (GSH), tris(2-carboxyethyl)phosphine (TCEP), or Dithiothreitol (DTT) can easily dissolve the hydrogel within minutes (Fig. 6A and B). Additionally, the hydrogel showed remarkable impermeability as it does not allow the movement of any molecule, including water, into or out of the gel. Moreover, a tightly knit fibrous network was observed in the gel matrix. We rationalised that, with the insolubility and unique confinement properties, PyKC-hydrogel could be an ideal candidate for the encapsulation and protection of enzymes. We assumed that the tightly knit network can encapsulate enzymes, restricting the space needed for them to unfold in response to external stimuli. Two different lipases were encapsulated within PyKC-hydrogel, and their catalytic performances were assessed in the presence of denaturing agents, including time (Fig. 6C), high temperature (Fig. 6D), urea and methanol (Fig. 6E), and change in pH (Fig. 6F). Interestingly, the encapsulated enzymes retained more than 75% activity while the free enzymes lost the activity completely under the influence of these denaturants. These results support that the PyKC hydrogel functions as a protective matrix for enzymes and other biomolecules, preserving their structural and catalytic function under destabilising conditions.

2.4.2. Platform for cell proliferation. The development of synthetic biomaterials for use in tissue engineering and regenerative medicine upholds academic and commercial significance.[97] The artificial ECM serves as a framework for cell adhesion and proliferation, thereby facilitating tissue regeneration.[98] Peptides are especially fascinating due to their natural compatibility with biological systems and non-cytotoxicity, along with a diverse array of functionalities that can be fine-tuned to develop the desired ECM-mimicking matrix. A significant amount of work has been conducted in the last few decades in this field.[64,99–101]

Fibrous proteins such as collagens, elastins, laminins, and fibronectins make various tissue-specific ECMs. The most widely used sequence is RGD, an integrin-binding peptide derived from fibronectin. Other cell-adhesive peptide (CAP) sequences employed to impart cell-adhesion properties include VAPG (elastin); YIGSR, KQAGDV, and REDV (fibronectin); LGTIPG, IKVAV, PDGSR, LRE, LRGDN, and IKLLI (laminin); and DGEA and GFOGER (collagen).

These CAPs are often incorporated with hydrogel-forming polymers to create composite hydrogels. The hydrogel network mimics the 3D structure of the ECM, while the CAPs allow effective cell binding. For example, Yang *et al.* developed an injectable hydrogel composed of chitosan, gelatin, β-glycerophosphate, and RGD peptide (**15**).[33] The RGD motif provides a favourable microenvironment for endothelial, smooth muscle, and mesenchymal stem cells. Loading stromal cell-derived factor 1 (SDF-1) and endothelial growth factor (VEGF) nanoparticles mimics ECM signalling and promotes angiogenesis. *In vitro* co-culture studies, chick embryo assays, and a rat myocardial infarction model demonstrated enhanced cell migration, blood vessel formation, and improved cardiac function, highlighting the potential of this approach for tissue engineering applications. In another work, Huang *et al.* developed a hydrogel film (ChT-PEDOT-p) by incorporating conductive

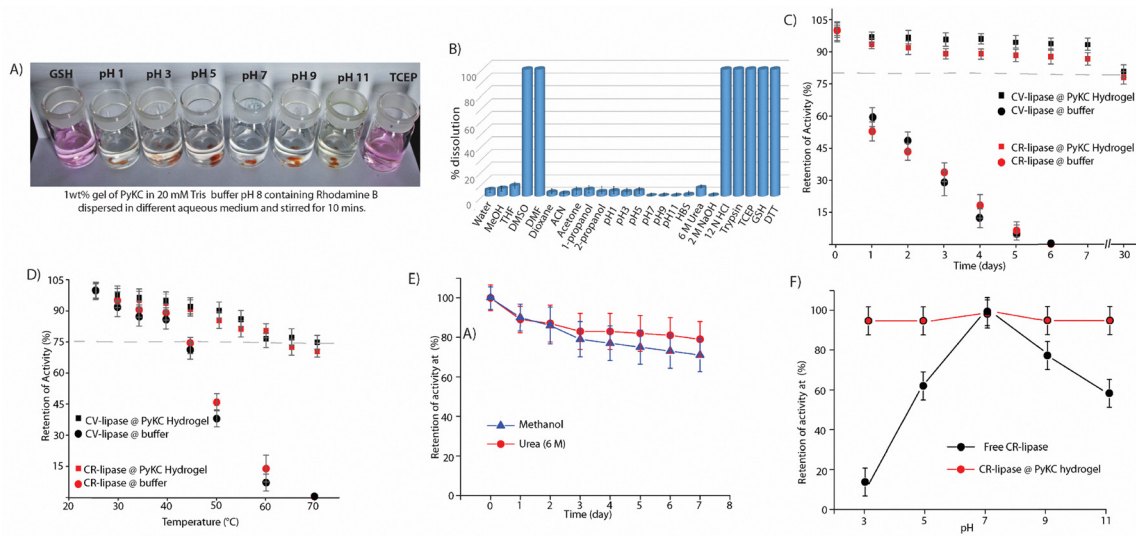

Fig. 6 (A) Photographs of vials containing different aqueous solutions where small portions of the hydrogel (1 wt% PyKC, **14**) containing rhodamine B were immerged and stirred for 10 min showing the insolubility of PyKC. (B) Percentage dissolution of a 1 wt% PyKC hydrogel (20 mM Tris-buffer, pH 8) in different media after 168 h. (C) Retention of the catalytic activities (%) of the gel-trapped and free enzymes at different time intervals when incubated at room temperature. (D) Retention of the catalytic activities (%) of CV and CR lipases as a function of temperature under PyKC hydrogel-trapped and free conditions. (E) Retention of activity (%) at different time intervals by the gel-trapped CR-lipase when dispersed in methanol or 6 M urea solutions. (F) Comparison of retention of activity by the CR-lipase under free and gel-trapped conditions when exposed to buffer solutions of different pH for 1 h. Reproduced from ref. 25 with permission. Copyright 2019, Royal Society of Chemistry.

poly(3,4-ethylenedioxythiophene) nanoparticles and the cell-adhesive tetrapeptide CRGD (**16**). The resulting film exhibited enhanced mechanical strength, supported Schwann cell attachment and proliferation, promoted vascularisation, and effectively induced regeneration of damaged sciatic nerves.[34] Since the shape and size of the polymer implemented is also important for their use as ECM, we hypothesised that multiple cross-linking strategies could offer a way to create cross-linked peptide-based polymers with adjustable shape and size. To this end, we have designed a peptide (**17**) with multiple possible cross-linking sites.[35] The peptide was cross-linked through disulfide linkages, horseradish peroxidase (HRP) -catalysed oxidation of Tyr units, and Cucurbit[8]uril (CB[8]) assisted supramolecular conjugation through FGG units. The crosslinked polymers demonstrated effective proliferation of RAW 264.7 macrophage cells, with 52.4 ± 5% greater efficiency compared to cells incubated for 48 hours.

Another short peptide segment from laminin commonly used to develop a synthetic cell proliferation platform is IKVAV (**18**). This peptide enhances neural regeneration, neuronal survival and maturation by binding to the β1-integrin subunit, thereby promoting the differentiation of neural progenitor cells into neurons. IKVAV-containing hydrogels have been shown to induce rapid neuronal and neurite differentiation. Jiang *et al.* developed a three-dimensional IKVAV-functionalized poly(lactide-ethylene oxide fumarate) (PLEOF) hydrogel, which exhibited excellent cell and tissue compatibility and supported the adhesion, proliferation, and differentiation of neural stem cells (NSCs) into neurons (Fig. 7A–C).[36] *In vivo* implantation for four weeks demonstrated good biocompatibility, highlighting its potential for spinal cord repair.

YIGSR (**19**), another pentapeptide with strong relevance to neural regeneration, has also been extensively investigated. Incorporation of YIGSR into composite hydrogels has been shown to enhance Schwann cell growth *in vitro* and promote sciatic nerve regeneration *in vivo* (Fig. 7A–D). Moreover, YIGSR-based anisotropic hydrogel micropatterns can effectively direct the alignment of Schwann cells.[102] Yang *et al.* further demonstrated that a bioactive YIGSR-based hydrogel catheter implanted into rat sciatic nerve gaps significantly promoted nerve regeneration, underscoring its therapeutic potential.[103]

Various natural polysaccharide-based hydrogels, such as chitosan (Cht), gelatin (Gel), hyaluronic acid (HA), and alginate (Alg), are widely utilised as scaffolds in the field of tissue engineering.[104] These materials meet the fundamental requirements of biocompatibility, hydrophilicity, and the ability to retain a large volume of water within their extensively entangled structure. However, they exhibit lower mechanical strength, rendering them weaker than the natural ECM and thus unsuitable for cell binding and differentiation. In this regard, we have incorporated our well-established PyKC (**14**) into these biopolymeric systems to design an ECM-mimicking matrix (Fig. 7E–G).[27] The ability of PyKC to create a very tightly woven network could improve the mechanical properties of the resulting hydrogels, rendering them a promising material for bone tissue engineering. The viability of the MC3 T3-E1 preosteoblast cells after 3 days of growth on the HA/PyKC hydrogel was found to be 85–90% based on the MTT assay, demonstrating the hydrogel's high biocompatibility. The extent of differentiation and matrix mineralization of these cells was also evaluated with Alizarin red assay. The cellular matrix exhibited a strong red stain after 14 days of differentiation on the HA/PyKC hydrogel (Fig. 7F). Quantification of the Alizarin red staining and alkaline phosphatase activity of the cells showed that the cells were grown efficiently on the matrix (Fig. 7G). Another library of peptides with the KC unit was evaluated for the ability of 3D cell culture. The screening of these peptides revealed that peptide **20** formed a suitable hydrogel matrix with the required rheological properties for 3D cell culture. We demonstrated that both differentiated RAW macrophages and undifferentiated THP-1 monocytes proliferated significantly within the 3D hydrogel matrix without exhibiting cytotoxic effects.[37]

Further, the efficient and unique hydrogelation by PyKC was explored to create an artificial cornea. A crosslinker-free supramolecular gelation strategy using PyKC and collagen was established.[28] In this system, collagen molecules were seamlessly integrated within the PyKC network without requiring any modification of the collagen. The resulting collagen implants (Coll-PyKC) were optically transparent, UV-blocking, mechanically robust, enzymatically stable, and amenable to suturing. Importantly, these implants supported the growth and function of all corneal cell types, promoted anti-inflammatory differentiation, and suppressed pro-inflammatory differentiation of human monocytes. In addition, they restricted the propagation of human adenoviruses.

2.4.3. Peptide hydrogels for drug delivery. Over the past few decades, soft materials such as self-assembled supramolecular hydrogels have garnered significant interest due to their potential applications in the fields of drug delivery and therapeutics.[8,64,101,105] However, although several reports have shown potential applications of these hydrogels for targeted drug delivery, the use of hydrogel-based delivery systems is currently restricted to topical applications.[3,64] To achieve localised sustained drug release within the body, these hydrogels must: (a) possess injectable properties (shear thinning); (b) maintain low solubility in biological fluids to prevent post-administration washout; (c) ensure biocompatibility; (d) release the therapeutic agent in response to specific stimuli that are elevated or expressed at the affected site. Developing systems that meet all these requirements is a challenging task. Several recent review articles provide comprehensive discussions of these issues for further reading.[8,106,107] In this section, we will focus solely on short peptide-based injectable systems used for the localised delivery of drugs.

Hydrogels formed from the hexapeptides H-FEFQFK-NH_2 (**21**) and H-FQFQFK-NH_2 (**22**), as reported recently by Madder *et al.* provide a versatile platform for sustained protein delivery.[38] Electrostatic interactions between the ionic peptide fibres and protein cargos strongly govern hydrogel formation, loading capacity, and release behaviour, enabling high protein loading while retaining thixotropic injectability and controlled release. Encapsulated enzymes preserve their activity during and after release. Notably, this injectable peptide hydrogel formulation of L-asparaginase for sustained delivery in a mouse model achieves a reduced initial bolus peak that may lower

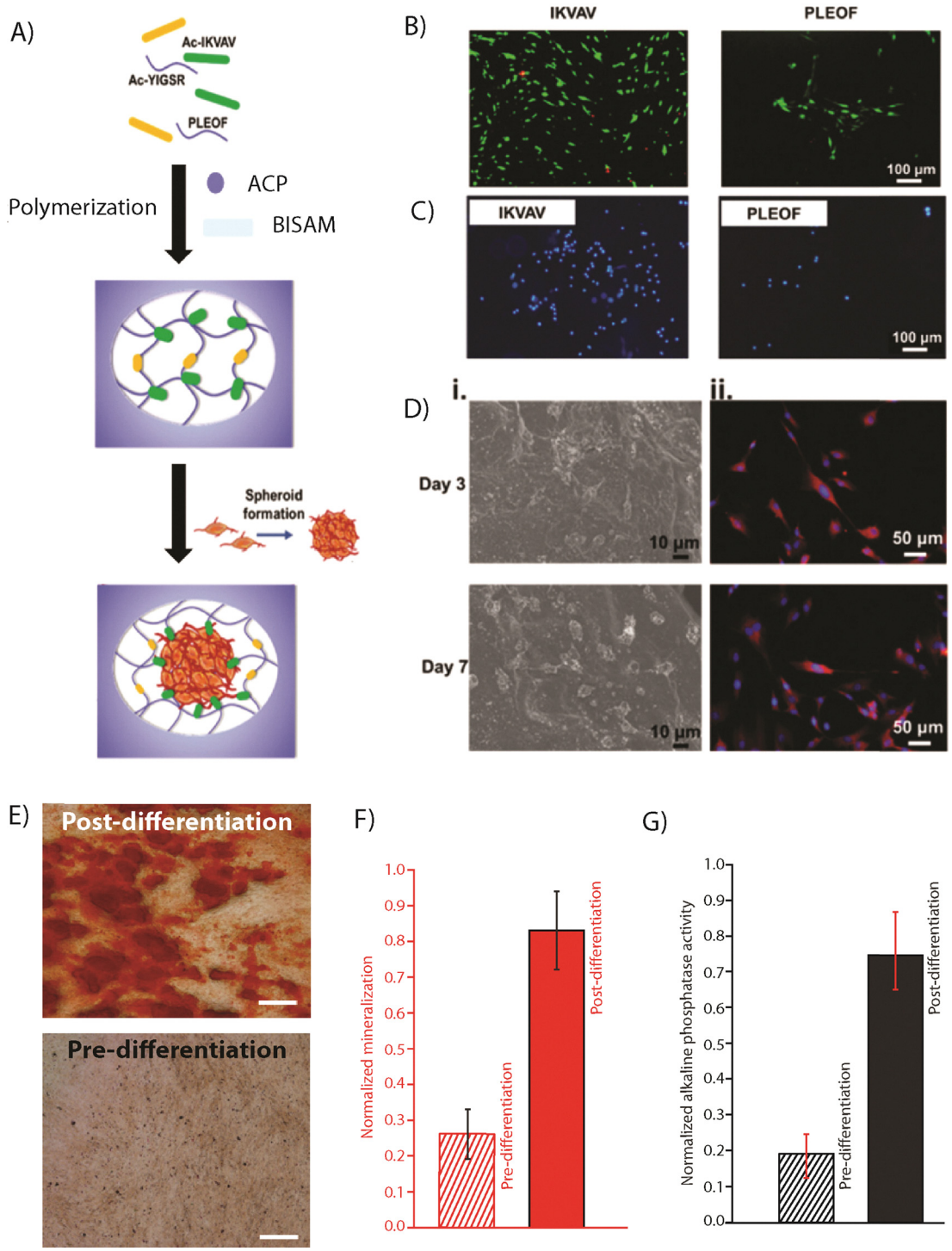

Fig. 7 (A)–(C) The neural stem cell attachment, growth, proliferation, and differentiation by IKVAV-PLEOF hydrogel. (A) Fabrication of the pre-gel mixture. Evaluation of cell viability (B), adhesion (C), and differentiation (D) on the IKVAV-PLEOF hydrogel surface. (E)–(G) Osteogenic response of MC3 T3-E1 cells on the HA/PyKC composite hydrogel. Adapted/reporduced with permission from ref. 27 and 36. Copyrights 2021 Royal Society of Chemistry and 2021 MDPI.

dose-related toxicity. With further optimisation of hydrogel erosion and cargo–matrix interactions to extend release times, this simple "mix-and-go" system holds broad potential for enzyme replacement therapies and cancer treatment applications. Another example is the work by Xing *et al.*, who exploited the composite thixotropic hydrogel formed by **13** and thiol-functionalized poly-L-lysine (PLL-SH) (Fig. 8A).[23] Due to its helical nanofibrous architecture, resembling fimbrial antigens, the hydrogel effectively activated T-cell responses and suppressed tumour growth in B16 melanoma mouse models. Treated mice

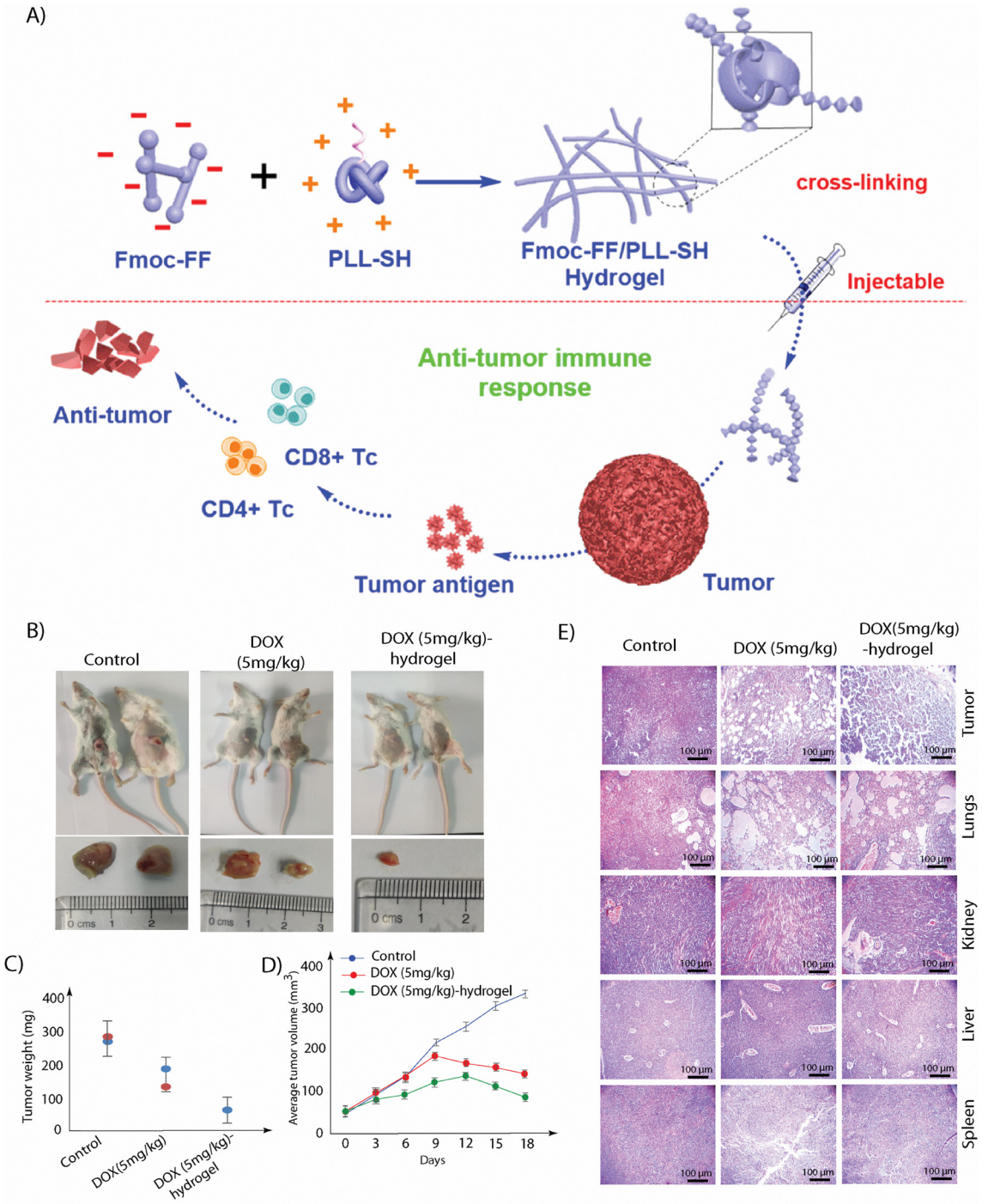

Fig. 8 (A) Schematic diagram of the formation of **13**/PLL-SH thixotropic hydrogel for drug delivery. (B)–(E) Effect of a single injection of DOX-loaded PyKC hydrogel. (B) Images of euthanized mice with tumors and isolated dissected tumors. (C) The weight of the tumors from different groups of mice. (D) The graph represents the volume of the dissected tumors at various time points during treatment. (E) Phase contrast microscopic images of tissues from different organs of the treated mice. The images are with 20× and 10× magnification. Reproduced and reproduced from ref. 23 and 26. Copyrights 217 American Chemical Society and 2019 Royal Society of Chemistry.

exhibited significantly elevated $CD4^+$, $CD8^+$, and $CD3^+$ T-cell populations. Overall, the chemical functionality of peptide hydrogels can modulate host immune responses, particularly during the early stages of inflammation. A new approach in this regard is to construct nucleobase-functionalized self-aggregating peptide hydrogels. Ade-FFF (**23**) self-assembles into a nano-fibrous injectable hydrogel. Doxorubicin (DOX) loaded Ade-FFF hydrogel showed a linear DOX release in response to proteinase K, and mice treated by injection of a DOX-containing Ade-FFF hydrogel showed a significant decrease in tumour size.[39]

In this regard, we observed that the PyKC (**14**) hydrogel fulfils all the criteria mentioned above for localised delivery. The hydrogel exhibited excellent thixotropic and injectable properties, enabling direct administration at the target tumour site. Its insolubility in HBS prevents leaching in biological fluids, while it has been found to be biocompatible and non-toxic. Owing to its unique confinement property, the encapsulated drug remains sequestered until the hydrogel network is disrupted.[25] Most importantly, the GSH responsiveness of the system makes it highly suitable for localised drug delivery, as elevated GSH levels in the tumour microenvironment facilitate a slow and sustained release of the trapped drug from the hydrogel matrix. Following this idea, DOX-loaded PyKC-hydrogel was injected directly on top of breast tumours in a mouse model, and the reduction in the tumour size was monitored (Fig. 8B).[26] Notably, the administration of a single dose of hydrogel containing DOX (5 mg kg^{-1}) resulted in significantly better tumour reduction (around 75% within 18 days, Fig. 8B–D) compared to the traditional treatment with doxorubicin alone and the control group. Furthermore, the persistent existence of the hydrogel containing the drug in proximity to the tumour for as long as 18 days post-administration emphasised its lasting efficacy. Additionally, no apparent side-effects were noticed on different organs like liver, kidney, lung and spleen (Fig. 8E). In general, this research emphasised the effectiveness and promise of the PyKC-hydrogel as a targeted drug delivery method for breast cancer therapy, setting the stage for future clinical uses and treatment strategies in oncology.

Despite tremendous advancements, several issues prevent self-assembled peptide-based biomaterials from being widely used in clinical settings. Due to their rapid clearance and susceptibility to enzymatic degradation, short peptides have limited *in vivo* stability, which can impair long-term functionality. The mechanical weakness of many peptide hydrogels prevents them from being used in load-bearing tissues unless they are reinforced or combined with other materials. Reproducibility and scalability may also be impacted by batch-to-batch variability and the sensitivity of self-assembly to slight variations in pH, ionic strength, or temperature. To improve proteolytic stability and mechanical robustness without compromising biocompatibility, sequence engineering and chemical modification are key components in the future of self-assembled peptides in biomedicine. It is anticipated that hybrid systems, which combine peptides with polymers, inorganic elements, or bioactive molecules, will produce multifunctional platforms with enhanced functionality. Peptides with predictable assembly and biological outcomes will be identified more quickly due to advancements in machine learning, high-throughput screening, and computational design. Crucially, closing the gap between laboratory innovation and clinical application will require a move toward *in vivo*-relevant models and translational research. With these advancements, self-assembled peptide systems have the potential to transform from sophisticated supramolecular structures into useful and significant biomedical materials.

2.5. Peptide-based catalytic scaffolds

The availability of different functional groups on the amino acid side chains makes the peptide nano-structures an attractive platform for catalysis. There are some excellent recent reviews available on peptide-assisted catalysis.[6,108,109] In this section, we will discuss some recent works in which peptide-based assemblies have been utilised as catalytic scaffolds.

2.5.1. Peptide nano-structures for catalysis. Over the last couple of decades, a significant amount of work has been conducted on catalysis by proline-based peptide aggregates. In one of the early examples, Clarke *et al.* have shown that proline–naphthyridine peptide conjugates can co-assemble *via* hydrogen bonding with pyridinones that can act as a catalyst for nitro-Michael addition reaction.[110] Escuder and group have shown that the lipopeptide ProValDoc (**24**) forms catalytically active hydrogels that can direct aldol reactions of aliphatic ketones with 4-nitrobenzaldehyde with improved selectivity (anti/syn 95 : 5) and the yield is dependent on the hydrophobicity of the ketone.[40] Hamley and coworkers have shown that the position of the Pro and the lipid chain in the lipopeptide plays a crucial role in the catalytic activity. Peptide, C_{16}-IKPEAP (**25**) forms spherical micelles with a disordered peptide conformation, whereas its reverse sequence, PAEPKI-C_{16} (**26**) assembles into β-sheet fibrils across a wide pH range. Peptide **26** exhibits higher conversion and improved anti: syn diastereoselectivity in a model nitro-aldol reaction.[41] Additionally, the peptide–lipid linker also affects catalysis. For example, although PRW-NH-C_{16} (amide, **27**) and PRW-O-C_{16} (ester, **28**) both form spherical micelles, the amide-linked lipopeptide shows enhanced catalytic activity, likely due to differences in local conformation or linker polarisation.[42]

By replicating the structural and functional features of enzymatic pockets that govern chemical transformations, it becomes possible to create enzyme mimics capable of performing similar reactions outside biological systems.For example, esterases utilise the Asp–Ser–His triad as the catalytic centre, and arranging such a triad in the peptide nanostructure can lead to an efficient esterase mimic. Following this strategy, a hydrolase-mimicking PA (**29**) has been reported, which shows stereoselective and repeatable enhanced catalysis.[43] The PA was designed by keeping the catalytic triad, along with an Arg residue that stabilises the catalytic pocket. Varying combinations of the amino acid positions and the tail length were analysed. The PA **29** was found to provide the highest catalytic activity. The branched peptide sequence, together with micelle formation, facilitated the three-dimensional organization of the catalytic triad, thereby enhancing substrate binding and improving catalytic performance through cooperative effects. The PA was further immobilised on a silica surface, and the PA-functionalized SiNP showed superior hydrolase activity compared to the free peptide as well as *Chromobacterium Viscosum* lipase (CV-lipase). Moreover, high stereoselective catalysis was observed, yielding 95% ee for the enantioselective hydrolysis of esters.

To this end, amyloid peptides are common in the field of catalysis. Simple, short amyloid peptides have been reported as

metalloprotease mimics. For example, Korendovych *et al.* analysed a library of seven residue peptides based on the "minimal" β-sheet sequence LKLKLKL with alternating hydrophobic and charged residues for the Zn^{2+}-dependent esterase-like activity. Lysine residues at positions 2 and 4 were replaced with histidine to enable Zn^{2+} binding and catalysis, while the influence of acidic, basic, or neutral residues at position 6 was systematically explored. The peptides form antiparallel β-strands that fold to coordinate Zn^{2+} ions, which act as catalytic cofactors and stabilise the β-sheet structure. Using pNPA as a substrate for ester hydrolysis, the peptide Ac-LHLHLQL-NH_2 (**30**) exhibited a Michaelis–Menten catalytic efficiency of $k_{cat}/K_M = 30 \pm 3\ M^{-1}\ s^{-1}$, exceeding that of carbonic anhydrase on a per-weight basis.[45] Similarly, another peptide, (**31**) containing a histidine and an alternating β-sheet-promoting sequence (HSGQQKFQFQFEQQ-NH_2), self-assembles into fibrils and exhibits esterase activity, which is further enhanced upon co-assembly with its arginine-containing analogue (H1R variant). The increased activity was attributed to the stabilisation of the substrate transition state by the arginine guanidinium group at the fibril binding site.[44]

Lynn's group utilised the KLVFF motif from the Aβ peptide and demonstrated that Ac-KLVFFAL-NH_2 (**32**) catalyses the retro-aldol cleavage of methodol to 6-methoxy-2-naphthaldehyde (Fig. 9). The peptide assembles into nanotubes in a water-acetonitrile mixture, with walls composed of antiparallel β-strands.[46] Catalytic activity was further probed by varying the cationic side chain length through substitution of Lysine with Ornithine, Arginine, and related residues. Reaction details, fluorescence-based product detection, initial rate data, and a model of methodol arrangement on the nanotube β-strand surface are illustrated in Fig. 9. The catalytic activities of short peptides were also explored in the context of transient catalysis and are discussed in Section 2.6

Short PAs have been used as templates to catalyse and control the shape, size and composition of nanostructures of various metals and silica. Templating peptide aggregates help cap metal nanoparticles and can enhance their catalytic activity. The formation of nano-fibrillar structures can be decorated with metal particles, which boost the catalytic activity. For example, the aniline functionalized peptide **33** readily self-assembles into positively charged fibrils, which were used to adsorb negatively charged citrate-functionalized Pt nanoparticles. The Pt-nanoparticle-coated fibrils were employed to modify the electrode, which exhibits high electrocatalytic activity towards oxygen reduction.[111]

Our group reported a simple lysine-containing PA **34** that self-assembles in water to form helical nanofibers, thereby forming a self-supporting hydrogel. The nanofibers were used as a template for the synthesis of silica, where the presence of free amine groups on the surface of the nanofibers acted as a

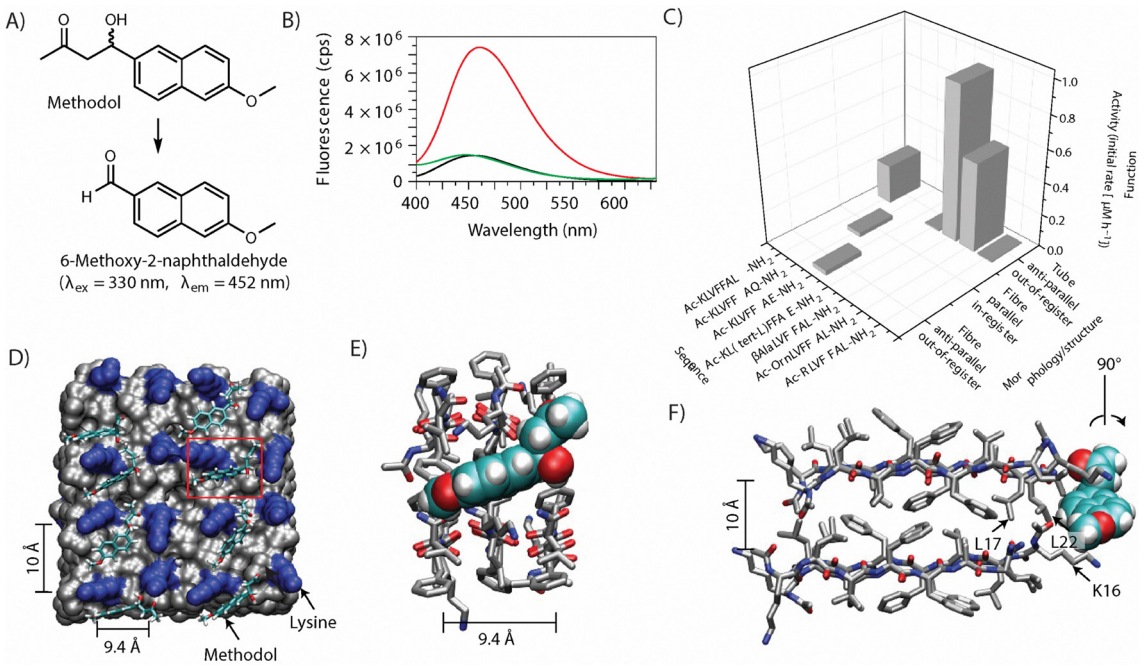

Fig. 9 (A) Retro-aldol reaction of (±)-methodol to generate the fluorescent 6-methoxy-2naphthaldehyde. (B) Fluorescence emission spectra (λ_{ex} = 330 nm) of 50 μM (±)-methodol (black line), 50 μM (±)-methodol with 1 mM Ac-KLVFFAL-NH_2 (**32**) nanotubes (red line), and 50 μM methodol with 1 mM Ac-RLVFFAL-NH_2 nanotubes (green line) incubated in 50 mM sodium phosphate buffer with 300 mM NaCl at pH 7.5 for 36 h at room temperature. Each sample contains 5% 6-methoxy-2-naphthaldehyde at zero time to establish baseline fluorescence. (C) Initial rate of production of 6-methoxy-2-naphthaldehyde by the indicated peptide assembly where the peptide concentration is 500 μM and the starting (±)-methodol concentration is 80 μM. (D) 1.2 ns molecular dynamics simulation of (*S*)-methodol docked onto the surface of K1 anti-parallel out-of-register amyloid assembly. In the space filling models the hydrophobic, LVFFAL residues are coloured grey, the lysines blue and methodol drawn as sticks with carbons coloured green, oxygen red and hydrogen white. (E) and (F) Expansions of methodol (space filling) on tube surface with peptides drawn as sticks. Adapted from ref. 46 with permission, copyright 2017, Springer Nature.

catalyst for the hydrolysis of tetraethoxysilane (TEOS) without the need for any additional reagent. The nano-fibre templates were removed by heating the samples at elevated temperature, leaving the hollow silica nanotubes.

2.5.2. Preparing hydrogel beads for catalytic conversions on the surface. In recent years, micro- and nanoscale spherical colloidal gel networks have garnered significant attention, as they retain essential gel-like characteristics, including high solvent content, tunable porosity, and the ability to encapsulate molecular cargo.[112] Additionally, they offer features such as large surface area, adjustable dimensions, and rapid responsiveness to external stimuli.[112,113] Furthermore, several studies have demonstrated that even bulk hydrogels can be engineered into defined shapes and sizes without compromising their inherent properties, thereby serving as versatile platforms for diverse applications such as ion and molecular recognition, oral drug delivery, tissue engineering, cell/protein encapsulation, and catalysis.[113] However, creating such macro-sized beads with supramolecular hydrogels is a challenging endeavour owing to their weak mechanical strength.

In this regard, Smith *et al.* reported a hybrid self-assembled microgel bead by combining a low-molecular-weight gelator and a calcium alginate polymer gelator. The hybrid beads contained interpenetrated networks formed by both the low-molecular-weight gelator and the polymer. The beads were prepared by an emulsion method, allowing the preparation of spherical gel particles of controllable sizes with diameters in the mm or μm range.[113] The microbeads were used for the delivery of bioactive agents. The same group also reported the preparation of core–shell hydrogel beads using the same gelator, using the extrusion method. In this case, the core was formed by the low-molecular-weight hydrogel, while the shell was prepared using calcium alginate.[114] Similarly, microfluidic techniques have been employed to fabricate microbeads from supramolecular hydrogels.[115]

Since the hydrogel beads are formed through the process of extrusion, emulsification or microfluidic technique, the hydrogels also need to be insoluble in bulk solvents and possess thixotropic properties. In this regard, PyKC (**14**) is a suitable candidate because of its unique properties as discussed in detail (Section 2.4.1). A rational approach was taken for the creation of a PyKC-based macro-sized gel bead using a simple extrusion method (Fig. 10).[30] To enhance the durability and applicability, the PyKC beads were further encased in a thin polymeric shell, thereby resulting in a core–shell configuration. The free Lysine groups on the surface of the beads enabled their easy modification. The beads were functionalised with dipentaerythritol penta-/hexa-acrylate (5ACl) and branched polyethylene imine (BPEI) alternatively, with the help of the well-known Michael addition. The possibility of keeping either acrylate or amine functionality on the surface of these beads allowed us to easily attach various functional groups and molecules to decorate the beads (Fig. 10). Utilizing the solubility of the PyKC-hydrogel (the core) in DMSO, treatment of these core–shell beads in this solvent resulted in hollow macro capsules (Fig. 10).

Exploiting the mild reducing property of BPEI, the BPEI-coated beads were surface decorated with gold nanoparticles (AuNPs), where no additional reducing agents were required. Nanoparticles of noble metals like gold has been of high interest because of its size and shape-dependent catalytic activities.[116] Utilising $NaBH_4$ as a hydrogen donor, the AuNPs acted as a catalyst for the reductive degradation of hazardous nitroaromatics. The work was further extended, where gold nanostars (AuNSs) were formed on the surface of the BPEI-coated beads, and their catalytic activity was analysed.[31] Gold nanostars are promising enzyme mimetic catalysts owing to their ability to interact with light and catalytic efficiency. Due to the localized surface plasmon resonance (LSPR), the BPEI-stabilized AuNSs showed remarkable photo-oxidase-like activity. LSPR, originating from the branched structure of the nanostars, enhanced the light absorption and further permitted the photo-induced catalytic processes. Its catalytic activity was then utilized in the detection and quantification of uric acid with the help of a colorimetric sensing assay. This technique worked on the strategy involving the oxidation of TMB in the presence of the AuNSs encapsulated core–shell beads, followed by its decoloration upon interacting with uric acid. AuNS@BPEI beads maintained their catalytic efficiency (approx. 70%) even after 10 cycles and an excellent detection limit of 6.2 μM. Additionally, using smartphone technology, a point-of-care testing (POCT) method was developed for real-time measurement. This increased the accessibility and convenience by enabling quick and precise on-site measurement of uric acid in urine and blood serum samples.

To this end, water remediation is a crucial field of research, as it has a direct impact on human health, ecosystems, and economic stability. Effective remediation ensures the availability of safe drinking water and reduces the burden of waterborne illnesses. Various approaches have been employed to address this issue, including peptide and protein-based systems.[117–119] We realised that the gold nanostructures and their catalytic activities can be fine-tuned through their preparation process. Thus, the presence of amine functionalities on the BPEI-coated beads can be used to create a negatively charged surface that alters the properties of the AuNS synthesised on it. The BPEI-coated core–shell bead was functionalized with 1,3-propanesultone solution, and the sulfate-functionalized surface allowed the formation of AuNS on the surface.[32] However, the AuNPs in this case showed non-plasmonic oxidase-like catalytic property. The AuNPs, confined to the bead surface, ensure rapid substrate access by eliminating diffusion barriers, thereby enabling efficient catalytic oxidation of a wide range of contaminants. The resulting AuNP@Beads exhibited excellent activity against phenolic pollutants, azo dyes, and biologically relevant catecholamines, including dopamine and epinephrine. In addition, they exhibited strong antibacterial efficacy against both Gram-negative and Gram-positive pathogens by generating reactive oxygen species. These catalytic beads are reusable, structurally stable under ionic stress, and exhibit negligible nanoparticle leaching. Importantly, wastewater treated with AuNP@Beads supports healthy plant growth, highlighting their environmental compatibility.

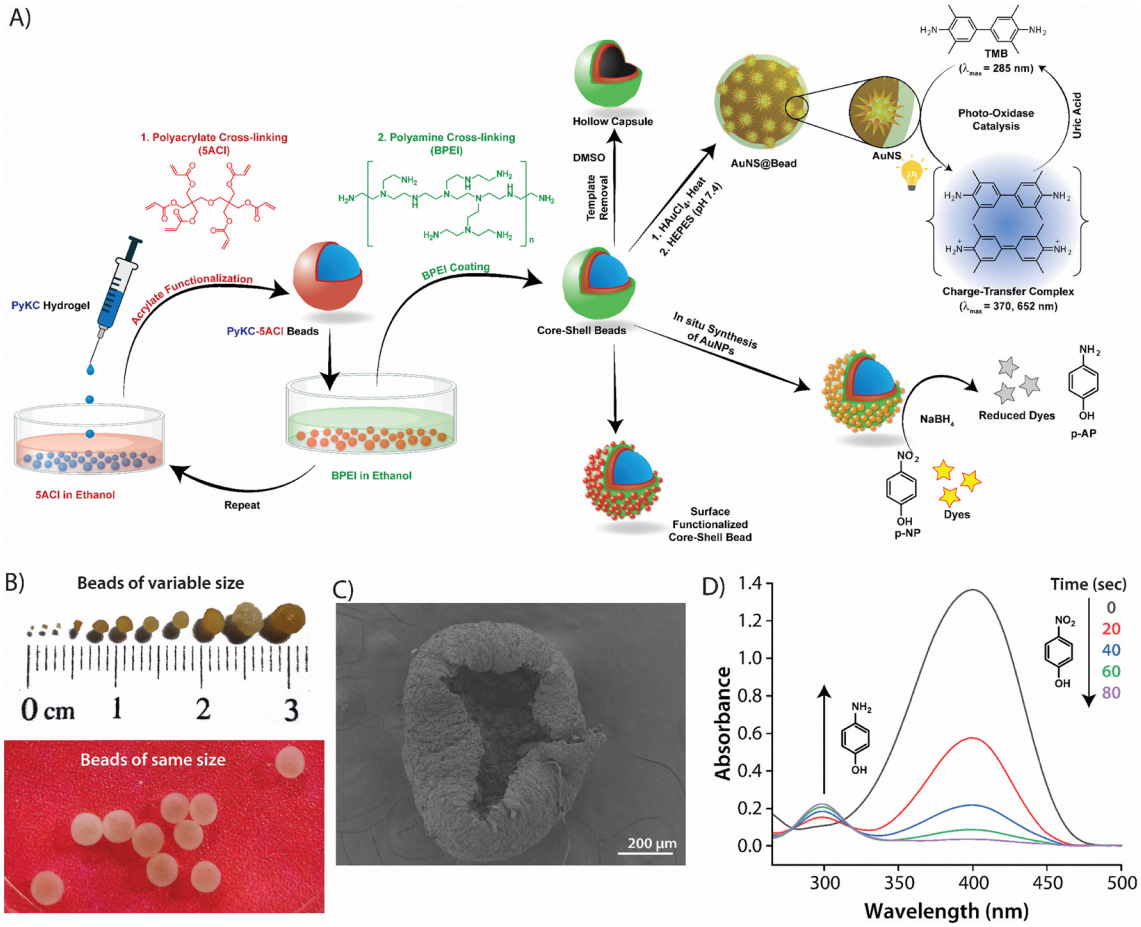

Fig. 10 (A) Schematic presentation of the stepwise formation of core–shell PyKC beads, hollow capsule, surface functionalized beads. The schematics also show the formation of gold nanoparticles (AuNS) and nanostars (AuNS) on the core–shell bead surface, as well as their catalytic reactions to reduce nitro-aromatics and exhibit photo-oxidase-like activity, respectively. (B) FESEM image of hollow capsule formed following the scheme depicted in (A). (C) Time dependent catalytic reduction of *p*-nitrophenol by AuNP@beads showing the efficacy of the systems to reduce nitro-aromatic dyes. (D) Catalytic reduction of different dyes by the AuNS-decorated sulfate functionalized core–shell beads. Reproduced from ref. 30 and 32. Copyright 2023 Elsevier and 2025 American Chemical Society.

Implementing this methodology, we gave shape, dimension, and durability to a peptide-based supramolecular hydrogel. Surfaces were modified effortlessly, allowing us to append desired functional groups, including those for complex systems like metallic nanoparticles. Besides convenient handling and repeatable cycles, we circumvented the chief problem associated with agglomeration in nanoparticles through this technique of immobilisation on hydrogel beads.

The applications of these peptide-derived catalytic scaffolds are, however, hindered by certain limitations. Firstly, they have lower efficiency compared to biocatalysts and metal ions, which often require less control over their precise structural configuration at the active site. Their instability against harsh reaction conditions (pH, temperature, and organic solvents), as well as susceptibility to proteolysis, further limits their use. Furthermore, it is also very difficult to obtain high specificity against their substrates and high reproducibility for their turnover number. Scaling up their synthesis can also prove to be very expensive. Future studies are, however, envisioned to ensure better rationalization of their sequences and introduction of a suitable secondary structure to better place their catalytic residues and enhance stability to active on-forms. Future breakthroughs can also arise through hybrid approaches by fusing these peptides-derived scaffolds either to metal ions/cofactors or to solid supports to greatly promote their efficiency and stability. The application of computational models, studies on directed evolution, and machine learning will also accelerate their discovery for high-efficiency motifs. With improved stability, efficiency, and scalability, peptide-based catalytic scaffolds have the potential to evolve into sustainable and tunable alternatives for next-generation catalytic applications.

2.6. Life-like materials using short peptides

Supramolecular aggregates exhibiting life-like attributes have emerged as a vibrant area of research over the past decade.[120–123] This relatively new field aims at designing biomimetic assemblies that obey the non-equilibrium thermodynamic pathways, which are central to biological assemblies. Introduction of a chemical trigger disrupts the equilibrium of a system, stimulating a chemical or environmental change that leads to the formation

of molecular assemblies. The assemblies are an outcome of the chemically triggered process and are maintained as long as the induced conditions persist. Once the chemical trigger is consumed, the assemblies are deactivated and disintegrate over time. It is worth mentioning that peptide-based self-assemblies have found a special place in unravelling the advanced spatio-temporal chemistry of chemically triggered and auto-regulated self-assemblies.[124,125]

These life-like attributes and adaptive systems can be achieved through the smart design of PAs, which can be built to respond to multiple stimuli as well. Thordarson and co-workers have demonstrated the kinetic control over the lifetime of a transient supramolecular hydrogel using a very simplistic design for a PA responsive to multiple stimuli. They have shown that a clear solution of anionic dibenzoyl cysteine (DBC^{2-}) can be triggered into gelation through the addition of an acid buffer containing TCEP (Fig. 11A).[48] Quick protonation of the pre-gelator solution led to DBC (**35**) formation and subsequent gelation. However, over time, TCEP reduced the disulfide bonds that disrupted the gel network, resulting in a sol of BC. Herein, the ultrashort PA was activated through a pH trigger but deactivated autonomously in the presence of a reducing agent. The lifespans of the transient hydrogel could be modulated by varying the pH or concentration of the reductant. The transient hydrogelation was also repeatable through reactivation of the solution over several cycles. In the context of dual stimuli, we observed that PyKC (**14**) contained the prerequisites needed to generate two orthogonally dynamic covalent linkages. The terminal Cys can form redox-responsive disulfides, while the side chain amine from Lys can participate in a pH-reversible imine bond. To construct a dual stimulus-responsive complex coacervate, we synthesised an aldehyde-functionalised water-soluble polymer (Poly-CHO).[29] When the polymer was combined with PyKC (below its CGC), turbidity appeared under basic pH due to complex coacervation initiated by dynamic covalent cross-linking from imine and disulfide bonds. The coacervates were highly adaptive towards any alterations in pH or redox conditions. The execution of pH clocks (TRIS:GdL) and redox clocks (H_2O_2/TCEP) produced transient coacervates with modulable lifetimes. The breaking of imine bonds under acidic conditions or disulfide cleavage under reductive environments dissolved the coacervates and inhibited LLPS.

Sometimes the assembly process can be driven by small molecules, whose consumption or dissipation over time can induce adaptive properties under non-equilibrium conditions. For example, a recent report has shown the formation of transient superstructures with PAs through activation with ATP (a biologically relevant small molecule) and deactivation through enzymatic consumption of ATP. They demonstrated that ATP aided the formation of β-sheet superstructures in a solution of polydisperse morphologies of $C_{16}V_3A_3K_3$ (**36**, Fig. 11B).[49] ATP provided proper charge screening and stabilised bundled nanofibers. Gradual enzymatic degradation of ATP by ATPase temporally disassembled the superstructures. Another popular method for creating transient peptide-based self-assemblies involves regulating the hydrophobicity of acidic side chain residues through carbodiimide chemistry. Boekhoven and coworkers have made significant contributions through their extensive work on PAs with terminal aspartic acid residues.[126–128] In this family of PAs, the addition of carbodiimide EDC generates active building blocks capable of supramolecular assemblies. The precursors are otherwise hydrophilic and fail to show assemblies. The terminal acid groups are locked into activated anhydride groups with EDC, which hydrophobized the overall molecule, enabling aggregations. These building blocks and their self-assembled structures were transiently formed as anhydrides were dissipated over time under a hydrolytic medium. A recent report utilising this chemistry has been put forward by Ahmed and coworkers employing an NMI functionalized ultrashort peptide amphiphile (NI-VD) (**37**, Fig. 12A).[50] When chemically fuelled with EDC, NI-VD formed NI-VD-An, which underwent hydrogelation. Entrapment of suitable energy acceptor dyes, such as DBT and NR, led to sequential energy transfer, resulting in multicolour gels with a transient nature under dissipative environments.

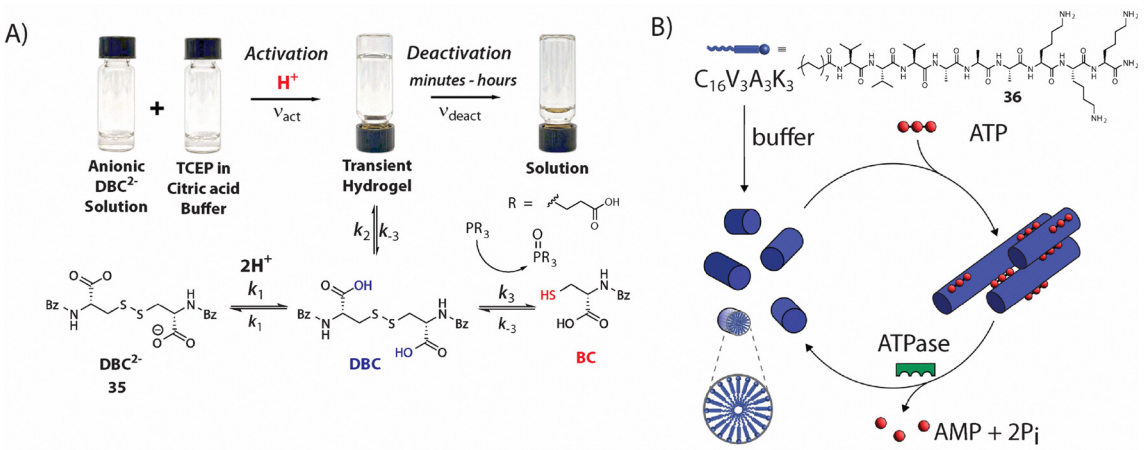

Fig. 11 Schematic representation of (A) kinetically controlled transient hydrogels with redox-reversible disulfide bond-based PA. (B) ATP-regulated assembly-disassembly of transient PA superstructures. Adapted from ref. 48, 49 Copyrights 2018, American Chemical Society; 2025 Wiley-VCH GmbH.

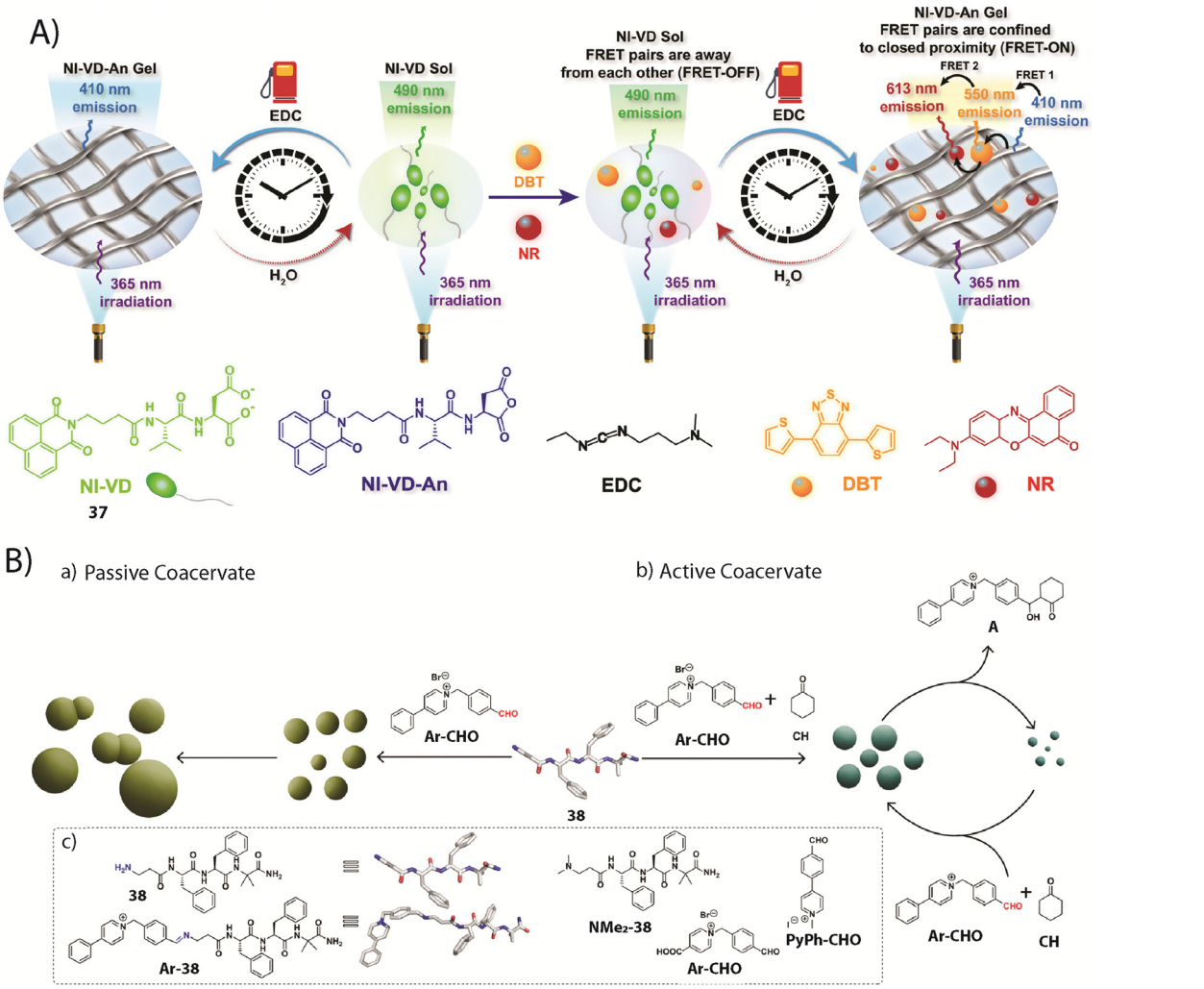

Fig. 12 (A) EDC-fueled time-gated luminescent transient hydrogels with multicolour emission. (B) Schematic representation showing the formation of (a) passive coacervate in the presence of **38** and Ar-CHO; and (b) active coacervate in the presence of **38**, Ar-CHO, and CH. (c) Chemical structures of peptide, *in situ* formed imine, control peptide, and aldehydes. Adapted from ref. 50, 51 Copyrights 2025 Wiley-VCH GmbH.

The multicoloured transient gels were further exploited in strategising information encryption techniques with anti-counterfeiting properties.

Since chemical fuels generate waste, repeatability is increasingly hindered by the accumulation of waste in chemically triggered systems over multiple cycles. The light-mediated assembly process is significant in this aspect. Generation of temporal properties through photo-responsive assemblies of PA is unique in its reproducibility. This can be achieved by integrating photo-responsive groups, such as spiropyran (SP) and azobenzene, into the design of PA. Such an example can be observed in the light-mediated gelation of a spiropyran-functionalized PA.[129] Normal conditions make the PA hydrophilic when the charged merocyanine (MC) form persists. Light-triggered MC to SP conversion provided a proper amphiphilic balance to the molecule, enabling the hydrogelation process. When irradiation was stopped, the molecule reverted to its equilibrium state, making the gel unstable again, and thus a transient gel was formed.

Over the past decade, Das and coworkers have rigorously investigated peptide-based assemblies to create temporally controlled functional nanostructures. They have thoroughly explored the non-equilibrium temporal regulation of catalytic and structural properties of active amyloid polymers based on short peptides.[130,131] In their most recent reports, they have demonstrated peptide-based catalytically active coacervates that are sustained out of equilibrium.[51] When a monocationic aldehyde (Ar-CHO) was mixed with a free amine containing a tetrapeptide (**38**, Fig. 12B) under basic conditions, it immediately formed passive coacervates after the generation of imine bonds in Ar-**38** (Fig. 12B). They showed coalescence with time. Active coacervates were obtained when the two components were mixed in the presence of cyclohexanone (CH). In this case, although large coacervates were produced immediately, they reduced in size over time and showed much lower coalescence. The free amine here catalyses the aldol condensation between CH and Ar-CHO through enamine reactions generated from the imines inside active droplets. This consumed a molecular

component necessary for the formation and sustenance of coacervates over time. Hence, the droplets reduced in size instead of coalescing. When CH and Ar-CHO were added in batches again, active coacervates with temporally dynamic dissolution and regeneration cycles were observed. Suppression of coalescence could modulate the lifetime of a system that demonstrated compartmentalisation along with intrinsic catalytic potential. The concept was also extrapolated into a more complex system that utilised similar chemistry to show demixing (phase separation) and dissolution of chiral coacervates under non-equilibrium conditions.[132] Here, active coacervates were formed from aromatic aldehydes containing esters and a free amine containing a tetrapeptide that exhibited enantioselective esterase activity. Active corcervates contained intrinsic catalytic properties that enabled them to cleave ester bonds, leading to the dissolution of droplets. Low-molecular-weight active coacervates provided a chiral microenvironment that facilitated kinetic resolution in chemical transformations, as observed in the dynamic nature of complex, membraneless organelles.

Supramolecular host–guest chemistry allows ample opportunities to create stimuli-responsive smart materials. However, this particular area is not very well explored for creating transient assemblies. We relied on the hetero-ternary complexation by CB[8] that lead to the formation of supramolecular peptide amphiphiles (SPA)and their vesicular aggregates.[133–137] First, we established a SPA, which was reversible with respect to an imine bond (Fig. 12A).[52] The SPA was constructed from two parts – an aldehyde-functionalized peptide-based head group and a long-chain aliphatic amine. The peptide head group was fully assembled by applying stable ternary complexation of CB[8] with the two aromatic guests – one functionalised with the aldehyde derivative (MV-CHO), while the other having the peptide head group (Nap-P, **39** Fig. 13A). The head group (Nap-P) contained a naphthalene unit as a guest for CB[8] appended to a hydrophilic sequence (GGGRGD) that could act as the polar head group. When a pH clock comprising urea-urease (a fast activator) and glucono-δ-lactone (GdL) (a slow deactivator) was initiated, the pH increased rapidly due to the release of ammonia from urea hydrolysis. This prompted the instantaneous formation of the imine bond between the two halves of the SPA, which assembled into vesicles. Saponification of GdL reduced the pH gradually over time, which caused the rupture of the dynamic covalent (imine) bonds.[138] The vesicular arrangement lost its integrity as the SPA disintegrated over time. The pH clock was repeated over multiple cycles, and time-programmable transient vesicles were formed. The temporal regulation of vesicles through host–guest chemistry has been rarely explored in this manner.

The work was further extended to create transient vesicles with more complex functionalities (Fig. 13B).[53] The head group of Nap-P was altered with GRSH (Nap-His, **41** Fig. 13B). This sequence is a well-reported catalytic triad that is capable of hydrolysing esters. A library of esters was studied as substrates, and a self-abolishing vesicle was created. The addition of alkaline TRIS buffer (pH 9.0, 1 mM) generated the vesicles.[139] The esters were hydrolysed at the surface of the vesicular nanozyme from the cooperative effect of catalytic triads in proximity. Hydrolysis of the esters released acids and phenols from various substrates (pNPA, pNPCAA and DNPA). The acids produced *in situ* were themselves responsible for pH reduction and disruption of vesicular aggregates. This is an example of biomimetic auto-regulation where products of a particular reaction inhibit their own production through negative feedback.

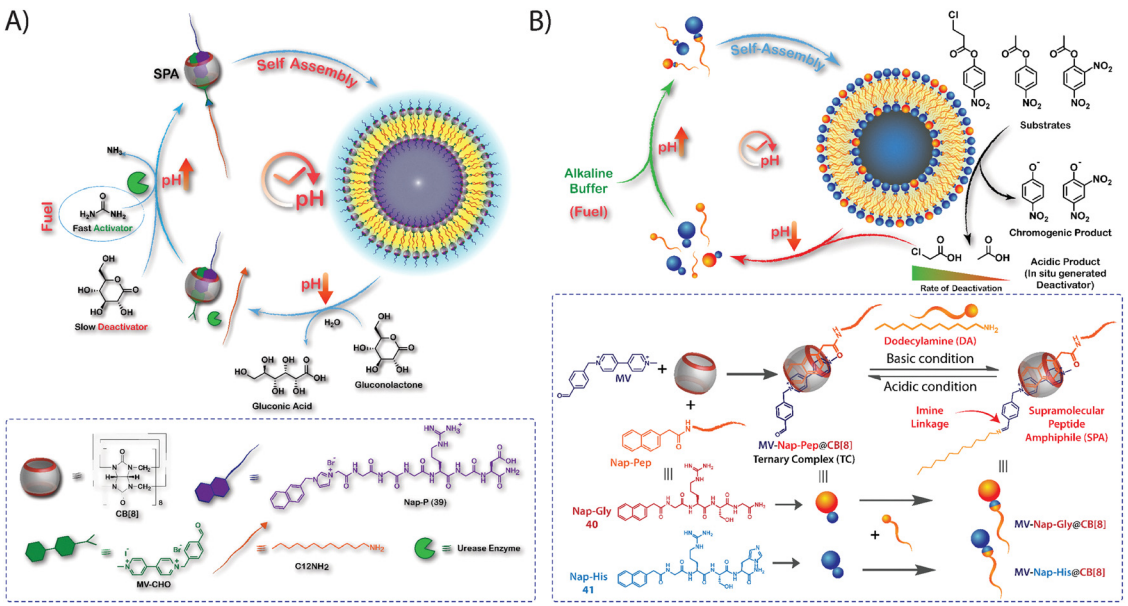

Fig. 13 Chemical structures and graphical presentation of (A) a pH-clock-driven temporal formation of a CB[8]-assisted SPA and its vesicles. (B) The formation of CB[8]-assisted SPA and the self-inhibitory feedback-driven temporal formation of nanozymes showing hydrolase-like catalytic activity. Reproduced from ref. 52 and 53. Copyrights 2019 and 2022 Royal Society of Chemistry.

The lifetime of the transient vesicles was controlled through the rate of catalytic activity and the hydrolytic propensity of the substrate studied. In a parallel study involving a similar system, a cascade reaction was investigated using a transient vesicle that followed a dual feedback loop.[140] A similar vesicular components were maintained, including a similar peptide sequence for hydrolase activity. The chemoenzymatic pH cycle consisted of a TRIS buffer as the activator and glucose-glucose oxidase (GOx) as the deactivator. The alkaline buffer triggered the formation of transient vesicular nanozymes. Hydrolysis of an ester of guaiacol produced hydrophobic guaiacol, which was effectively sequestered in the vesicular bilayer. The vesicles were activated in the presence of Hemin, which was also retained preferentially in the bilayer. In the same system, the enzymatic oxidation of glucose generated gluconic acid as the deactivator and H_2O_2 as the by-product. The H_2O_2 promoted the oxidative formation of tetraguaiacol from guaiacol by the peroxidase activity of hemin, while the gluconic acid lowered the pH to disrupt the vesicles. This peptide-based nanozyme demonstrated several complex life-like features. They include *in situ* generation of deactivator leading to self-regulating vesicles, tandem reactions where the product of one reaction (H_2O_2 and guaiacol) serves as the reactant for another (peroxidase), bidirectional positive (through H_2O_2) and negative (through gluconic acid) feedback loop operated in controlling both the lifetime and kinetics, nano-compartmentalisation through selective sequestration in a hydrophobic domain. All these attributes enabled the vesicles to act as tandem nanozymes, exhibiting selectivity, enhanced activity, substrate specificity, and repeatability, similar to cellular systems. The strategy employed here, using pH-responsive PA, can be extended to combine incompatible catalysts in multicompartment nanozymes for efficient one-pot tandem transformations.

These studies suggest that peptide-functionalized assemblies can be rationally designed to generate innovative, adaptive, and life-like systems. Beyond exhibiting contemporary biomimetic characteristics, such platforms offer valuable insight into early evolutionary processes by employing biologically relevant, primitive molecular building blocks. While recreating truly life-like behaviour remains a distant goal due to the inherent complexity of living systems, current advances represent an important first step. With continued technological progress and the integration of machine-learning–driven design, the future of this field appears highly promising.

Conclusions and outlook

This review underscores the significant potential of self-assembled short peptides across diverse applications. Effective application-specific design requires a clear understanding of the intended use, followed by careful selection and positioning of amino acids within the peptide sequence to meet those requirements. In sensing applications, the ligand and chromophore are arranged such that analyte binding induces a measurable spectral change. Likewise, for catalysis, the display of catalytic motifs on the surface of ordered peptide assemblies is crucial, as this organisation enables efficient catalysis through a persistently high density of functional sites. For tissue engineering and 3D cell culture, the aggregation of the peptides must fulfil the criteria of forming a three-dimensional network mimicking the ECM, and the sequences should be designed in a way to effectively adhere the cells. It has been a long-standing goal of supramolecular chemists to create self-assembled systems in which molecules can be arranged to allow for the directed and controlled flow of electrons. Small peptide-based systems hold high potential in the field of organic electronics. However, the goal is yet to be achieved. In drug delivery, injectable hydrogel systems that resist dissolution in biofluids and respond to local biological cues are essential for effective *in vivo* performance, and advances in peptide design increasingly enable these requirements to be met. Finally, the emerging field of life-like systems illustrates how small peptides can be precisely tailored to form dissipative, transient assemblies.

In the era of AI and ML, future research is likely to be highly impacted by AI and ML in a positive way. Reports are surfacing on artificial intelligence-driven approaches for the rational design of peptides with predictable aggregation propensity.[61,62] With advanced ML tools, combined with input from state-of-the-art computational modelling, it will be easier to predict, design, and prepare new peptides for targeted applications. The applications will no longer be restricted to the one mentioned in this article. Rather, we can expect applications in several new fields. For instance, energy storage and battery technologies are areas where peptides have seen limited presence so far. However, the emerging catalytic efficiency of peptide-based aggregates suggests that small peptides could become viable components in such systems. These small peptides often face significant challenges related to stability, cellular uptake, and overall bioavailability. While individual modifications may not adequately address all these limitations, macrocyclisation could be one powerful strategy capable of simultaneously enhancing affinity, selectivity, proteolytic stability, and membrane permeability.[141] In this regard, AI and ML-based tools could be of significant help, as they will enable the easy identification of biocompatible sequences and their modifications. Another major concern is the scalability of these peptides. Scaling peptide production from milligram to kilogram scales entails many technical and operational challenges. However, with newer technologies like microwave-assisted peptide synthesis, contract development & manufacturing organisations (CDMOs) across the world are handling this issue successfully. Overall, supported by accumulated knowledge and advancing technologies, small peptide-based systems hold a promising future.

Conflicts of interest

The authors declare that they have no conflict of interest.

Data availability

There is no data related to the article that can be shared.

Acknowledgements

DD acknowledges BRNS, India (58/14/05/2022), for financial assistance. PD and MKB want to thank PMRF, India, for research fellowships.

References

1 T. N. Das, A. Ramesh, A. Ghosh, S. Moyra, T. K. Maji and G. Ghosh, *Nanoscale Horiz.*, 2025, **10**, 279–313.
2 N. J. Sinha, M. G. Langenstein, D. J. Pochan, C. J. Kloxin and J. G. Saven, *Chem. Rev.*, 2021, **121**, 13915–13935.
3 P. Das and D. Das, in *Peptide Bionanomaterials: From Design to Application*, ed. M. A. Elsawy, Springer, Cham, 2023, pp. 145–194.
4 A. Levin, T. A. Hakala, L. Schnaider, G. J. L. Bernardes, E. Gazit and T. P. J. Knowles, *Nat. Rev. Chem.*, 2020, **4**, 615–634.
5 R. Chang, C. Yuan, P. Zhou, R. Xing and X. Yan, *Acc. Chem. Res.*, 2024, **57**, 289–301.
6 I. W. Hamley, *Biomacromolecules*, 2021, **22**, 1835–1855.
7 L. Adler-Abramovich and E. Gazit, *Chem. Soc. Rev.*, 2014, **43**, 6881–6893.
8 S. Guo, J. Wang, Q. Wang, J. Wang, S. Qin and W. Li, *Heliyon*, 2024, **10**, e26009.
9 P. Wang, J. Wu, C. Di, R. Zhou, H. Zhang, P. Su, C. Xu, P. Zhou, Y. Ge, D. Liu, W. Liu and Y. Tang, *Biosens. Bioelectron.*, 2017, **92**, 602–609.
10 L. N. Neupane, E.-T. Oh, H. J. Park and K.-H. Lee, *Anal. Chem.*, 2016, **88**, 3333–3340.
11 B. Pramanik, N. Singha and D. Das, *ACS Appl. Polym. Mater.*, 2019, **1**, 833–843.
12 N. Singh, S. Sharma, R. Singh, S. Rajput, N. Chattopadhyay, D. Tewari, K. B. Joshi and S. Verma, *Chem. Sci.*, 2021, **12**, 16085–16091.
13 B. Pramanik, S. Ahmed, N. Singha and D. Das, *ChemistrySelect*, 2017, **2**, 10061–10066.
14 B. Pramanik, S. Das and D. Das, *Chem. – Asian J.*, 2020, **15**, 4291–4296.
15 N. Singha, P. Gupta, B. Pramanik, S. Ahmed, A. Dasgupta, A. Ukil and D. Das, *Biomacromolecules*, 2017, **18**, 3630–3641.
16 P. Das, S. Routray, M. K. Baroi, T. Das and D. Das, *Anal. Chem.*, 2025, **97**, 10628–10637.
17 V. Nguyen, R. Zhu, K. Jenkins and R. Yang, *Nat. Commun.*, 2016, **7**, 13566.
18 J. Hu, W. Kuang, K. Deng, W. Zou, Y. Huang, Z. Wei and C. F. J. Faul, *Adv. Funct. Mater.*, 2012, **22**, 4149–4158.
19 S. Ahmed, K. N. Amba Sankar, B. Pramanik, K. Mohanta and D. Das, *Langmuir*, 2018, **34**, 8355–8364.
20 S. Ahmed, B. Pramanik, K. N. A. Sankar, A. Srivastava, N. Singha, P. Dowari, A. Srivastava, K. Mohanta, A. Debnath and D. Das, *Sci. Rep.*, 2017, **7**, 9485.
21 N. Singha, S. Neogi, B. Pramanik, S. Das, A. Dasgupta, R. Ghosh and D. Das, *ACS Appl. Polym. Mater.*, 2019, **1**, 2267–2272.
22 O. Ben-Zvi, I. Grinberg, A. A. Orr, D. Noy, P. Tamamis, I. Yacoby and L. Adler-Abramovich, *ACS Nano*, 2021, **15**, 6530–6539.
23 R. Xing, S. Li, N. Zhang, G. Shen, H. Möhwald and X. Yan, *Biomacromolecules*, 2017, **18**, 3514–3523.
24 N. Singha, B. K. Das, B. Pramanik, S. Das and D. Das, *Chem. Sci.*, 2019, **10**, 10035–10039.
25 N. Singha, A. Srivastava, B. Pramanik, S. Ahmed, P. Dowari, S. Chowdhuri, B. K. Das, A. Debnath and D. Das, *Chem. Sci.*, 2019, **10**, 5920–5928.
26 S. Halder, T. Das, R. Kushwaha, A. K. Misra, K. Jana and D. Das, *Mater. Horiz.*, 2025, **12**, 987–1001.
27 S. Chowdhuri, M. Ghosh, L. Adler-Abramovich and D. Das, *Pharmaceutics*, 2021, **13**, 1602.
28 M. M. Islam, A. Chivu, D. B. AbuSamra, A. Saha, S. Chowdhuri, B. Pramanik, C. H. Dohlman, D. Das, P. Argüeso, J. Rajaiya, H. K. Patra and J. Chodosh, *Sci. Rep.*, 2022, **12**, 9108.
29 S. Chowdhuri, S. Das, R. Kushwaha, T. Das, B. K. Das and D. Das, *Chem. – Eur. J.*, 2023, **29**, e202203820.
30 T. Das, S. Das and D. Das, *Chem. Eng. J.*, 2023, **477**, 147105.
31 T. Das, S. Das and D. Das, *J. Mater. Chem. B*, 2025, **13**, 1079–1088.
32 T. Das, M. Yadav, S. Das, G. Mondal, S. Chatterjee and D. Das, *Langmuir*, 2025, **41**, 25439–25453.
33 Y. Ding, A.-s Zhao, T. Liu, Y.-n Wang, Y. Gao, J.-a Li and P. Yang, *Ann. Biomed. Eng.*, 2020, **48**, 1511–1523.
34 L. Huang, X. Yang, L. Deng, D. Ying, A. Lu, L. Zhang, A. Yu and B. Duan, *ACS Appl. Mater. Interfaces*, 2021, **13**, 16106–16117.
35 P. Dowari, S. Saha, B. Pramanik, S. Ahmed, N. Singha, A. Ukil and D. Das, *Biomacromolecules*, 2018, **19**, 3994–4002.
36 Y. Yin, W. Wang, Q. Shao, B. Li, D. Yu, X. Zhou, J. Parajuli, H. Xu, T. Qiu, A. K. Yetisen and N. Jiang, *Biomater. Sci.*, 2021, **9**, 2887–2892.
37 S. Chowdhuri, A. Saha, B. Pramanik, S. Das, P. Dowari, A. Ukil and D. Das, *Langmuir*, 2020, **36**, 15450–15462.
38 H. Vu, E. Peeters, K. Hofkens, K. Vandemeulebroecke, S. T'Sas, C. Martin, S. Ballet, R. Hoogenboom, S. Goossens, T. Lammens, M. Van Trimpont and A. Madder, *Biomater. Sci.*, 2025, **13**, 4139–4152.
39 K. Baek, A. D. Noblett, P. Ren and L. J. Suggs, *Biomater. Sci.*, 2020, **8**, 3130–3137.
40 N. Singh and B. Escuder, *Chem. – Eur. J.*, 2017, **23**, 9946–9951.
41 J. N. B. D. Pelin, C. J. C. Edwards-Gayle, V. Castelletto, A. M. Aguilar, W. A. Alves, J. Seitsonen, J. Ruokolainen and I. W. Hamley, *ACS Appl. Mater. Interfaces*, 2020, **12**, 13671–13679.
42 V. Castelletto, C. J. C. Edwards-Gayle, I. W. Hamley, J. N. B. D. Pelin, W. A. Alves, A. M. Aguilar, J. Seitsonen and J. Ruokolainen, *ACS Appl. Mater. Interfaces*, 2019, **2**, 3639–3647.
43 P. Dowari, M. Kumar Baroi, T. Das, B. Kanti Das, S. Das, S. Chowdhuri, A. Garg, A. Debnath and D. Das, *J. Colloid Interface Sci.*, 2022, **618**, 98–110.
44 C. Zhang, X. Xue, Q. Luo, Y. Li, K. Yang, X. Zhuang, Y. Jiang, J. Zhang, J. Liu, G. Zou and X.-J. Liang, *ACS Nano*, 2014, **8**, 11715–11723.
45 C. M. Rufo, Y. S. Moroz, O. V. Moroz, J. Stöhr, T. A. Smith, X. Hu, W. F. DeGrado and I. V. Korendovych, *Nat. Chem.*, 2014, **6**, 303–309.
46 T. O. Omosun, M.-C. Hsieh, W. S. Childers, D. Das, A. K. Mehta, N. R. Anthony, T. Pan, M. A. Grover, K. M. Berland and D. G. Lynn, *Nat. Chem.*, 2017, **9**, 805–809.
47 S. Ahmed, J. H. Mondal, N. Behera and D. Das, *Langmuir*, 2013, **29**, 14274–14283.
48 J. P. Wojciechowski, A. D. Martin and P. Thordarson, *J. Am. Chem. Soc.*, 2018, **140**, 2869–2874.
49 D. Cappelletti, F. Lancia, A. Basagni and L. Đorđević, *Small*, 2025, **21**, 2410850.
50 S. Ahmed, S. A. Islam, M. K. Baroi, B. K. Das and B. Pramanik, *Adv. Mater.*, 2025, **37**, e09789.
51 S. Bal, S. Gupta, C. Mahato and D. Das, *Angew. Chem., Int. Ed.*, 2025, **64**, e202505296.
52 P. Dowari, S. Das, B. Pramanik and D. Das, *Chem. Commun.*, 2019, **55**, 14119–14122.
53 S. Das, T. Das, P. Das and D. Das, *Chem. Sci.*, 2022, **13**, 4050–4057.
54 S. Han, S. Cao, Y. Wang, J. Wang, D. Xia, H. Xu, X. Zhao and J. R. Lu, *Chem. – Eur. J.*, 2011, **17**, 13095–13102.
55 J. P. Schneider, D. J. Pochan, B. Ozbas, K. Rajagopal, L. Pakstis and J. Kretsinger, *J. Am. Chem. Soc.*, 2002, **124**, 15030–15037.
56 A. Dasgupta and D. Das, *Langmuir*, 2019, **35**, 10704–10724.
57 H. Barzinmehr, S. Ramezanpour, P. Shiri, E. Meghrazi Ahadi, S. Mohammadi, F. Yazdian and P. Tavatoni, *Coord. Chem. Rev.*, 2024, **518**, 216055.
58 M. C. Lucana, Y. Arruga, E. Petrachi, A. Roig, R. Lucchi and B. Oller-Salvia, *Pharmaceutics*, 2021, **13**, 2065.
59 P. Dowari, B. Pramanik and D. Das, *Bull. Mater. Sci.*, 2020, **43**, 70.
60 Q. Chen, G. Liu, M. Li and K. Zhang, *Chem. – Eur. J.*, 2025, **31**, e01968.
61 S. Yang, J. Ren, W. Gao, L. Cao and S. Ling, *npj Soft Matter*, 2025, **1**, 4.
62 E. Dražić, D. Jelušić, P. Janković Bevandić, G. Mauša and D. Kalafatovic, *ACS Nano*, 2025, **19**, 20295–20320.
63 L. Li, R. Zheng and R. Sun, *Macromol. Biosci.*, 2025, **25**, 2400523.
64 S. Das and D. Das, *Front. Chem.*, 2021, **9**, 770102.
65 J. Krämer, R. Kang, L. M. Grimm, L. De Cola, P. Picchetti and F. Biedermann, *Chem. Rev.*, 2022, **122**, 3459–3636.
66 W. J. Tipping, L. T. Wilson, S. K. Blaseio, N. C. O. Tomkinson, K. Faulds and D. Graham, *Chem. Commun.*, 2020, **56**, 14463–14466.
67 G. Klös, M. Miola and D. S. Sutherland, *J. Phys. Chem. C*, 2019, **123**, 7347–7355.
68 D. Das, A. Dasgupta, S. Roy, R. N. Mitra, S. Debnath and P. K. Das, *Chem. – Eur. J.*, 2006, **12**, 5068–5074.

69 P. Singh, A. Hirsch and S. Kumar, *Trends Anal. Chem.*, 2021, **138**, 116237.
70 B. Pramanik, J. H. Mondal, N. Singha, S. Ahmed, J. Mohanty and D. Das, *ChemPhysChem*, 2017, **18**, 245–252.
71 B. Pramanik, S. Ahmed, R. Roy, B. K. Das, N. Singha and D. Das, *ChemistrySelect*, 2017, **2**, 8911–8916.
72 E. Kondo, H. Iioka and K. Saito, *Cancer Sci.*, 2021, **112**, 2118–2125.
73 B. Chang, J. Chen, J. Bao, T. Sun and Z. Cheng, *Chem. Rev.*, 2023, **123**, 13966–14037.
74 S. J. Barrow, S. Kasera, M. J. Rowland, J. del Barrio and O. A. Scherman, *Chem. Rev.*, 2015, **115**, 12320–12406.
75 D. Das and O. A. Scherman, *Isr. J. Chem.*, 2011, **51**, 537–550.
76 D. Das, K. I. Assaf and W. M. Nau, *Front. Chem.*, 2019, **7**, 619.
77 Z.-Y. Zhang and Y. Liu, *Chem. Sci.*, 2019, **10**, 7773–7778.
78 S. Ahmed, N. Singha, B. Pramanik, J. H. Mondal and D. Das, *Polym. Chem.*, 2016, **7**, 4393–4401.
79 K. Tao, P. Makam, R. Aizen and E. Gazit, *Science*, 2017, **358**, eaam9756.
80 N. Amdursky, M. Molotskii, E. Gazit and G. Rosenman, *J. Am. Chem. Soc.*, 2010, **132**, 15632–15636.
81 Z. Gan, X. Wu, X. Zhu and J. Shen, *Angew. Chem., Int. Ed.*, 2013, **52**, 2055–2059.
82 L. Adler-Abramovich, D. Aronov, P. Beker, M. Yevnin, S. Stempler, L. Buzhansky, G. Rosenman and E. Gazit, *Nat. Nanotechnol.*, 2009, **4**, 849–854.
83 M. Yemini, M. Reches, J. Rishpon and E. Gazit, *Nano Lett.*, 2005, **5**, 183–186.
84 C. Li and H. Wonneberger, *Adv. Mater.*, 2012, **24**, 613–636.
85 Y. Tidhar, H. Weissman, S. G. Wolf, A. Gulino and B. Rybtchinski, *Chem. – Eur. J.*, 2011, **17**, 6068–6075.
86 A. Srivastava, A. Garg, D. Das and A. Debnath, *Bull. Mater. Sci.*, 2020, **43**, 181.
87 B. Pramanik, S. Ahmed, N. Singha, B. K. Das, P. Dowari and D. Das, *Langmuir*, 2019, **35**, 478–488.
88 H. C. Ates, P. Q. Nguyen, L. Gonzalez-Macia, E. Morales-Narváez, F. Güder, J. J. Collins and C. Dincer, *Nat. Rev. Mater.*, 2022, **7**, 887–907.
89 R. Kushwaha, S. Dey, K. Gupta, B. B. Mandal and D. Das, *ACS Appl. Mater. Interfaces*, 2024, **16**, 5183–5195.
90 R. L. Baldwin, *J. Mol. Biol.*, 2007, **371**, 283–301.
91 L. R. Engelking, in *Textbook of Veterinary Physiological Chemistry*, ed. L. R. Engelking, Academic Press, Boston, 3rd edn, 2015, pp. 18–25.
92 K. Jiang, L. S. Schadler, R. W. Siegel, X. Zhang, H. Zhang and M. Terrones, *Mater. Chem.*, 2004, **14**, 37–39.
93 S. Ganguli, K. Yoshimoto, S. Tomita, H. Sakuma, T. Matsuoka, K. Shiraki and Y. Nagasaki, *J. Am. Chem. Soc.*, 2009, **131**, 6549–6553.
94 J. M. Beierle, K. Yoshimatsu, B. Chou, M. A. Mathews, B. K. Lesel and K. J. J. A. C. I. E. Shea, *Angew. Chem., Int. Ed.*, 2014, **53**, 9275–9279.
95 X. Huang, J. Li, Y. Araki, T. Wada, Y. Xu and M. Takai, *RSC Adv.*, 2024, **14**, 18807–18814.
96 J. Zhang, J. C. White, G. V. Lowry, J. He, X. Yu, C. Yan, L. Dong, S. Tao and X. Wang, *Nat. Commun.*, 2025, **16**, 3050.
97 D. M. Ryan and B. L. Nilsson, *Polym. Chem.*, 2012, **3**, 18–33.
98 G. Huang, F. Li, X. Zhao, Y. Ma, Y. Li, M. Lin, G. Jin, T. J. Lu, G. M. Genin and F. Xu, *Chem. Rev.*, 2017, **117**, 12764–12850.
99 H. Cao, L. Duan, Y. Zhang, J. Cao and K. Zhang, *Signal Transduction Targeted Ther.*, 2021, **6**, 426.
100 W. Li, J. Hu, C. Chen, X. Li, H. Zhang, Y. Xin, Q. Tian and S. Wang, *Regen. Ther.*, 2023, **24**, 459–471.
101 A. Dasgupta, J. H. Mondal and D. Das, *RSC Adv.*, 2013, **3**, 9117–9149.
102 G. Li, S. Li, L. Zhang, S. Chen, Z. Sun, S. Li, L. Zhang and Y. Yang, *ACS Appl. Mater. Interfaces*, 2019, **11**, 37397–37410.
103 S. Chen, Y. Zhao, X. Yan, L. Zhang, G. Li and Y. Yang, *J. Biomed. Mater. Res., Part A*, 2019, **107**, 1273–1283.
104 X. Xue, Y. Hu, Y. Deng and J. Su, *Adv. Funct. Mater.*, 2021, **31**, 2009432.
105 P. Dowari, S. Roy, S. Das, S. Chowdhuri, R. Kushwaha, B. K. Das, A. Ukil and D. Das, *Chem. – Asian J.*, 2022, **17**, e202200550.
106 D. Berillo, A. Yeskendir, Z. Zharkinbekov, K. Raziyeva and A. Saparov, *Medicina*, 2021, **57**, 1209.
107 W. Xiao, W. Jiang, Z. Chen, Y. Huang, J. Mao, W. Zheng, Y. Hu and J. Shi, *Signal Transduction Targeted Ther.*, 2025, **10**, 74.
108 L. R. Marshall, O. Zozulia, Z. Lengyel-Zhand and I. V. Korendovych, *ACS Catal.*, 2019, **9**, 9265–9275.
109 K.-Y. Wang, J. Zhang, Y.-C. Hsu, H. Lin, Z. Han, J. Pang, Z. Yang, R.-R. Liang, W. Shi and H.-C. Zhou, *Chem. Rev.*, 2023, **123**, 5347–5420.
110 M. L. Clarke and J. A. Fuentes, *Angew. Chem., Int. Ed.*, 2007, **46**, 930–933.
111 B. Zhou, Z. Sun, D. Li, T. Zhang, L. Deng and Y.-N. Liu, *Nanoscale*, 2013, **5**, 2669–2673.
112 Y. B. Hamzah, S. Hashim and W. A. W. A. Rahman, *J. Polym. Res.*, 2017, **24**, 134.
113 C. C. Piras, A. G. Kay, P. G. Genever and D. K. Smith, *Chem. Sci.*, 2021, **12**, 3958–3965.
114 C. C. Piras, P. Slavik and D. K. Smith, *Angew. Chem., Int. Ed.*, 2020, **59**, 853–859.
115 S. Bai, S. Debnath, K. Gibson, B. Schlicht, L. Bayne, M. Zagnoni and R. V. Ulijn, *Small*, 2014, **10**, 285–293.
116 M. Azharuddin, G. H. Zhu, D. Das, E. Ozgur, L. Uzun, A. P. F. Turner and H. K. Patra, *Chem. Commun.*, 2019, **55**, 6964–6996.
117 B. K. Das, B. Pramanik, S. Chowdhuri, O. A. Scherman and D. Das, *Chem. Commun.*, 2020, **56**, 3393–3396.
118 M. Peydayesh and R. Mezzenga, *Nat. Commun.*, 2021, **12**, 3248.
119 N. Wichmann, R. Gruseck and M. Zumstein, *Environ. Sci. Technol.*, 2024, **58**, 717–726.
120 A. Jain, S. Dhiman, A. Dhayani, P. K. Vemula and S. J. George, *Nat. Commun.*, 2019, **10**, 450.
121 S. Maiti, I. Fortunati, C. Ferrante, P. Scrimin and L. J. Prins, *Nat. Chem.*, 2016, **8**, 725–731.
122 J. Boekhoven, W. E. Hendriksen, G. J. M. Koper, R. Eelkema and J. H. van Esch, *Science*, 2015, **349**, 1075–1079.
123 M. Kumar, N. L. Ing, V. Narang, N. K. Wijerathne, A. I. Hochbaum and R. V. Ulijn, *Nat. Chem.*, 2018, **10**, 696–703.
124 A. Chatterjee, A. Reja, S. Pal and D. Das, *Chem. Soc. Rev.*, 2022, **51**, 3047–3070.
125 F. Sheehan, D. Sementa, A. Jain, M. Kumar, M. Tayarani-Najjaran, D. Kroiss and R. V. Ulijn, *Chem. Rev.*, 2021, **121**, 13869–13914.
126 X. Chen, M. A. Würbser and J. Boekhoven, *Acc. Mater. Res.*, 2023, **4**, 416–426.
127 P. S. Schwarz, M. Tena-Solsona, K. Dai and J. Boekhoven, *Chem. Commun.*, 2022, **58**, 1284–1297.
128 X. Chen, B. A. K. Kriebisch, A. M. Bergmann and J. Boekhoven, *Chem. Sci.*, 2023, **14**, 10176–10183.
129 M. Liu, C. N. Creemer, T. J. Reardon and J. R. Parquette, *Chem. Commun.*, 2021, **57**, 13776–13779.
130 S. Goswami, A. Reja, S. Pal, A. Singh and D. Das, *J. Am. Chem. Soc.*, 2022, **144**, 19248–19252.
131 S. Bal, C. Ghosh, P. Parvin and D. Das, *Nano Lett.*, 2023, **23**, 9988–9994.
132 S. Gupta, S. Jha, C. Mahato and D. Das, *Nat. Commun.*, 2025, **16**, 9336.
133 Y. J. Jeon, P. K. Bharadwaj, S. Choi, J. W. Lee and K. Kim, *Angew. Chem., Int. Ed.*, 2002, **41**, 4474–4476.
134 D. Jiao, J. Geng, X. J. Loh, D. Das, T.-C. Lee and O. A. Scherman, *Angew. Chem., Int. Ed.*, 2012, **51**, 9633–9637.
135 J. H. Mondal, T. Ghosh, S. Ahmed and D. Das, *Langmuir*, 2014, **30**, 11528–11534.
136 J. H. Mondal, S. Ahmed and D. Das, *Langmuir*, 2014, **30**, 8290–8299.
137 J. H. Mondal, S. Ahmed, T. Ghosh and D. Das, *Soft Matter*, 2015, **11**, 4912–4920.
138 B. Pramanik and D. Das, *J. Phys. Chem. C*, 2018, **122**, 3655–3661.
139 P. Das, T. Das, S. Koley, M. Kumar Baroi, S. Das, J. Mohanty and D. Das, *Angew. Chem., Int. Ed.*, 2025, **64**, e202414239.
140 S. Das, P. Das, P. Dowari, B. K. Das and D. Das, *J. Colloid Interface Sci.*, 2022, **614**, 172–180.
141 J. He, P. Ghosh and C. Nitsche, *Chem. Sci.*, 2024, **15**, 2300–2322.